N73-20683

THE PENNSYLVANIA
STATE UNIVERSITY

CASE FILE
COPY

SPIN REORIENTATION OF A NONSYMMETRIC BODY WITH ENERGY DISSIPATION

BY

ROBERT J. CENKER

ASTRONAUTICS RESEARCH REPORT

NO. 73-2

DEPARTMENT OF AEROSPACE ENGINEERING
UNIVERSITY PARK, PENNSYLVANIA

RESEARCH SUPPORTED BY NASA GRANT NGR 39-009-162

ACKNOWLEDGMENTS

The author wishes to acknowledge the assistance of his advisor, Dr. Marshall H. Kaplan, Associate Professor of Aerospace Engineering, for suggesting the problem and for his encouragement through the course of the investigation. He would also like to express his appreciation to his fellow graduate students for their assistance and encouragement.

This investigation was made possible by the sponsorship of the National Aeronautics and Space Administration under NASA Grant NGR 39-009-162.

TABLE OF CONTENTS

LIST OF FIGURES

LIST OF SYMBOLS

A, C	fluid slug moments of inertia
$\tilde{d}_1 \tilde{d}_2 \tilde{d}_3$	unit vectors along principal body axis
D	diameter of ring cross section
f	Darcy-Wiesbach resistance coefficient
$\tilde{h}$	angular momentum vector in body fixed co-ordinates
$\tilde{H}$	angular momentum vector in inertial co-ordinates
I_1, I_2, I_3	principal moments of inertia
m	mass of each moving mass
N_3	moment due to viscous shear in ring
P	circumference of ring cross section
r, R	parameters of moving mass system, defined in Figure 8
R_{ad}	mean radius of viscous ring
R_n	Reynolds number
T	rotational kinetic energy
$\dot{\alpha}$	angular velocity of fluid slug relative to the damper ring
ν, ρ	kinematic viscosity and density of damper, respectively
τ_o	shear stress
$\tilde{\omega}$	angular velocity vector of the satellite
ψ, θ, ϕ	Euler's angles

Subscripts

A, B	after and before weight shift, respectively
a, b	above and below the separatrix, respectively
u, ℓ	upper and lower limits, respectively

INTRODUCTION

It is a well documented fact that rotating semi-rigid bodies ("rigid" bodies experiencing energy dissipation) are stable only when the rotation is about the axis of maximum moment of inertia. This has been demonstrated analytically,[1] and verified in flights such as Explorer I[2] and ATS-V[3] satellites. The problem arises from the two potential orientations which the final spin vector can take after large angle reorientation from minor to major axis, i.e., along the positive or negative axis of the maximum inertia. Reorientation of a satellite initially spinning about the minor axis using an energy dissipation device may require that the final spin orientation be controlled. Examples of possible applications are the Apogee Motor Assembly with Paired Satellites (AMAPS) configuration,[4] where proper orientation of the thruster is required; and reorientation of ATS-V, where the spin sensitive nature of the despin device ('yo-yo' mechanism) requires that the final spin vector point in a specified direction. The primary purpose of this work is to investigate techniques for eliminating such spin orientation ambiguities through active controls. This control capability would be useful in controlling orientation of tumbling bodies for retrieval purposes, and for actively reorienting spin stabilized satellites which could be initially spun up by the launch vehicle (either earth launch or shuttle deployment) about the minor axis of inertia.

SUMMARY OF PAST WORK

Effects of energy dissipation on satellite dynamics have been experienced in actual flights[2,3,5] and discussed in several analytical treatments.[1,6,7,8,9] These efforts, have, in general, dealt with discussions of the effect of dissipation on the precession rates and the total time required for a satellite to go from one spin state to another. References 1 and 6 describe attitude drift for single and dual-spin symmetric bodies. Reference 7 discusses the effect of flexible appendages as energy dissipators on symmetric satellite dynamics. Non-symmetric body motion in body fixed and inertial coordinates is discussed in Reference 8 while Reference 9 illustrates several methods of modeling the energy dissipation process and describes effects on non-symmetric bodies.

Control of attitude drift is discussed in References 10, 11, and 12. Axisymmetric spacecraft control is proposed in Reference 10, in which a method is presented for maintaining a satellite on a configuration other than spinning about the axis of maximum inertia. This is done by addition of energy into the system to compensate for energy dissipation. Reference 11 touches briefly on non-symmetric satellite precession control with controlled energy dissipation, and presents numerical examples for symmetric satellites. Control of a non-symmetric satellite is studied in Reference 12, but only for small nutation angles, i.e., active energy dissipation is used to return the satellite to the desired stable position after it has been perturbed. None of the control systems proposed to date have considered the

question of whether the spin vector will align itself with the positive or negative axis of maximum moment of inertia when the spin axis is initially about the minor axis.

DYNAMICS ANALYSIS

Constant energy motion of a non-symmetric, rigid body, in a torque-free environment is geometrically described by Poinsot's motion. This is the motion of an inertia ellipsoid (having dimensions proportional to the moments of inertia of the body) that rolls without slipping on an "invariable plane" while its center is a fixed distance $\sqrt{2T/H}$ from the plane.[9] This situation is illustrated in Figure 1. The allowable paths for this motion in the body fixed coordinate frame are closed curves called polhodes, each having a fixed discrete energy level for given angular momentum. Figure 2 shows several polhodes on the inertia ellipsoid for a fixed angular momentum and several different energy levels.

A logical extension of this motion for dissipative bodies is a change in the distance from the center of the ellipsoid to the invariable plane, resulting in a continuous change in polhode curves. Figure 3 illustrates this process along with a geometric interpretation of the critical point of the tumbling motion, i.e., whether $\tilde{\omega}$ has a positive or negative component along $\tilde{d}_3$ when the energy passes $H^2/2I_2$ determines the final spin orientation.

Since the nutation angle θ (instantaneous position of the $\tilde{d}_3$ axis with respect to the angular momentum vector) is the parameter of concern, equations giving θ as a function of time and/or rotational energy are desirable. Although the equations of motion for a non-symmetric body are elliptical in nature and, therefore, not readily reduced to an analytic solution, limits on the nutation angle can be developed as straightforward functions of the energy state. For

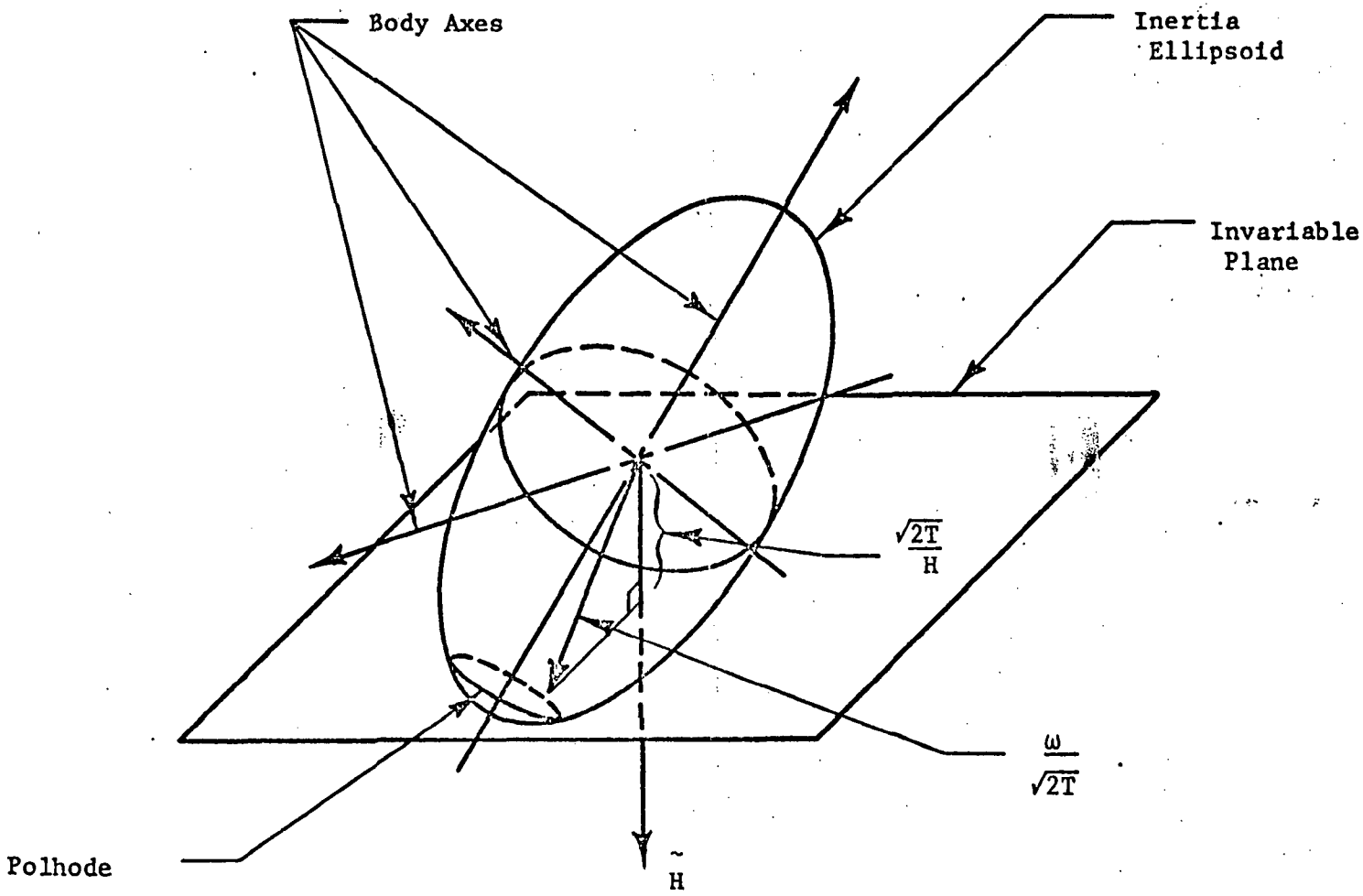

Figure 1. Rigid Body Poinsot Motion

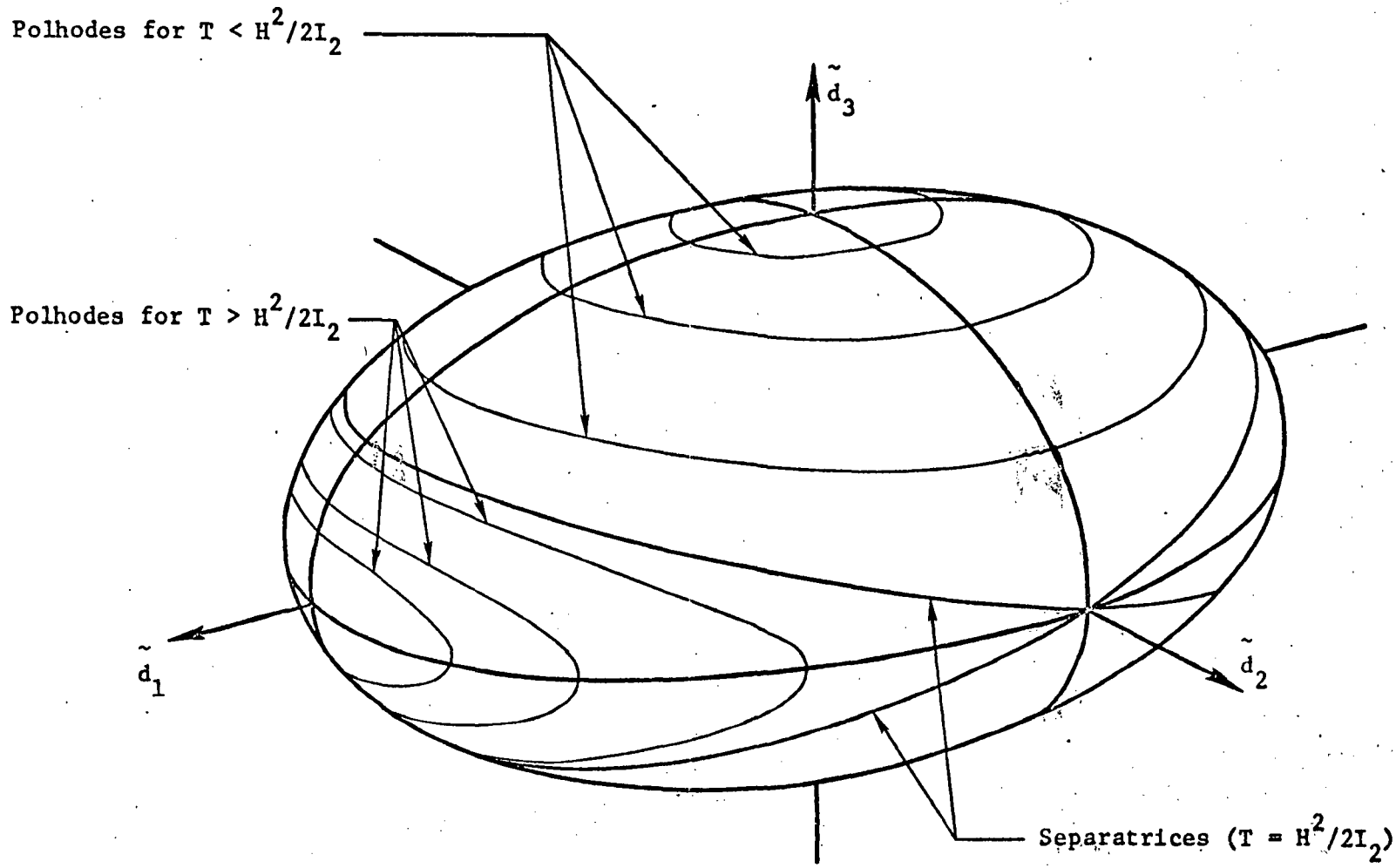

Figure 2. Rigid Body Polhodes

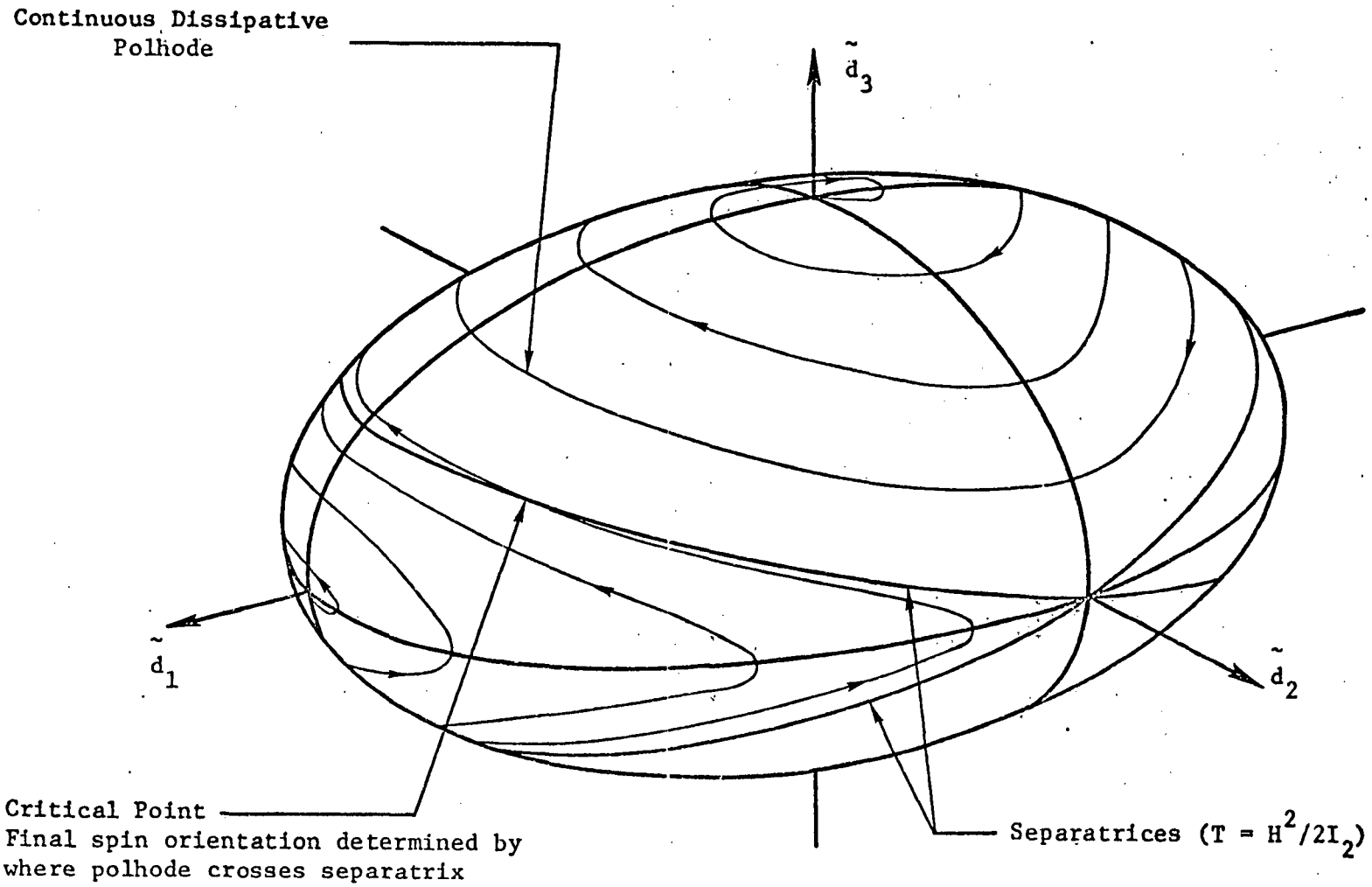

Figure 3. Dissipative Body Polhode

$T < H^2/2I_2$, Reference 9 develops these bounds in the following manner. Extreme values of θ exist when $\tilde{\omega}$ lies in either the 2-3 or 1-3 plane, as explained in Appendix A and illustrated in Figure 4. This results in the angular momentum and energy taking on the following values:

at θ_u	at θ_ℓ
$H^2 = I_2^2\omega_2^2 + I_3^2\omega_3^2$	$H^2 = I_1^2\omega_1^2 + I_3^2\omega_3^2$
$2T = I_2\omega_2^2 + I_3\omega_3^2$	$2T = I_1\omega_1^2 + I_3\omega_3^2$

From the geometry of the situation, it is evident that

$$\sin^2\theta_u = \frac{I_2^2\omega_2^2}{H^2} \qquad \sin^2\theta_\ell = \frac{I_1^2\omega_1^2}{H^2}$$

$$= \frac{I_2}{H^2}(2T - I_3\omega_3^2) \qquad = \frac{I_1}{H^2}(2T - I_3\omega_3^2)$$

$$= \frac{I_2}{I_3H^2}(2I_3T - H^2 + I_2^2\omega_2^2) \qquad = \frac{I_1}{I_3H^2}(2I_3T - H^2 + I_1^2\omega_1^2)$$

Manipulation of these equations leads to

$$\sin^2\theta_u = \frac{I_2(2I_3T-H^2)}{H^2(I_3-I_2)} + \frac{I_2^2}{I_3H^2(I_3-I_2)}\{-2I_3T + H^2 + I_2\omega_2^2(I_3-I_2)\}$$

$$\sin^2\theta_\ell = \frac{I_1(2I_3T-H^2)}{H^2(I_3-I_1)} + \frac{I_1^2}{I_3H^2(I_3-I_1)}\{-2I_3T + H^2 + I_1\omega_1^2(I_3-I_1)\}$$

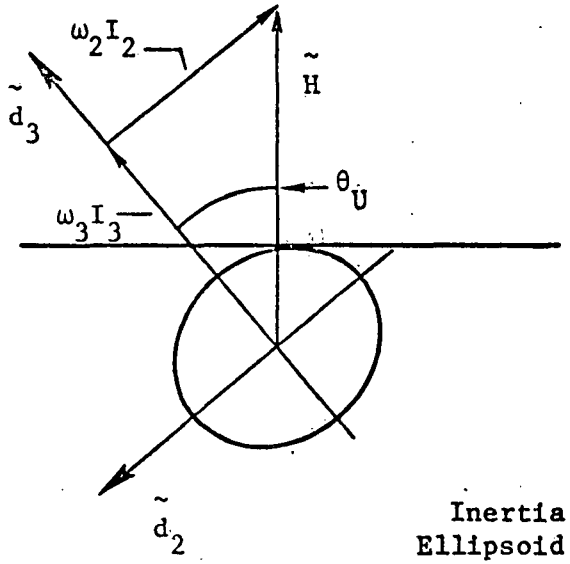

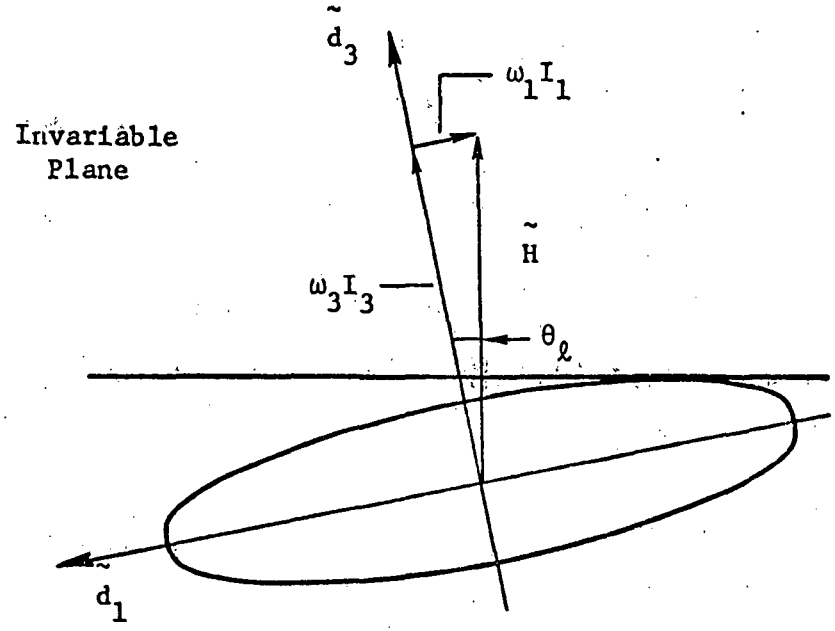

θ_u = Upper limit on nutation angle

θ_ℓ = lower limit on nutation angle

Figure 4. Inertia Ellipsoid Orientation at Extreme Values of θ

Keeping in mind the particular energy and momentum conditions that exist at the respective extremes, the terms in brackets reduce to zero, leaving

$$\sin^2\theta_u = \frac{I_2(2I_3T-H^2)}{H^2(I_3-I_2)}$$

$$\sin^2\theta_\ell = \frac{I_1(2I_1T-H^2)}{H^2(I_3-I_1)}$$

With the energy above the separatrix level ($T > H^2/2I_2$) the following parallel development can be made. Figure 5 shows the inertia ellipsoid with the $\tilde{d}_3$ axis in one of its extreme positions. As ω_1 never equals zero (the elliptic solution for ω_1 with $T > H^2/2I_2$ never changes sign[13]), the upper and lower limits must both exist where ω_2 equals zero. At this point ω_1 and ω_3 determine the nutation angle θ. For a given energy state, every zero of the ω_2 function coincides with the same value for ω_1, with ω_3 having the same absolute value but alternating sign. Thus the $\tilde{d}_3$ axis must oscillate about 90° with the maximum angle of the oscillation giving both the upper and lower bounds on θ. Defining this angle as θ_{ex} results in the following equations:

$$\sin^2\theta_{ex} = \frac{I_3^2\omega_3^2}{H^2} = \frac{I_3}{H^2}(2T - I_1\omega_1^2)$$

$$= \frac{I_3}{I_1H^3}(2I_1T - H^2 + I_3\omega_3^2)$$

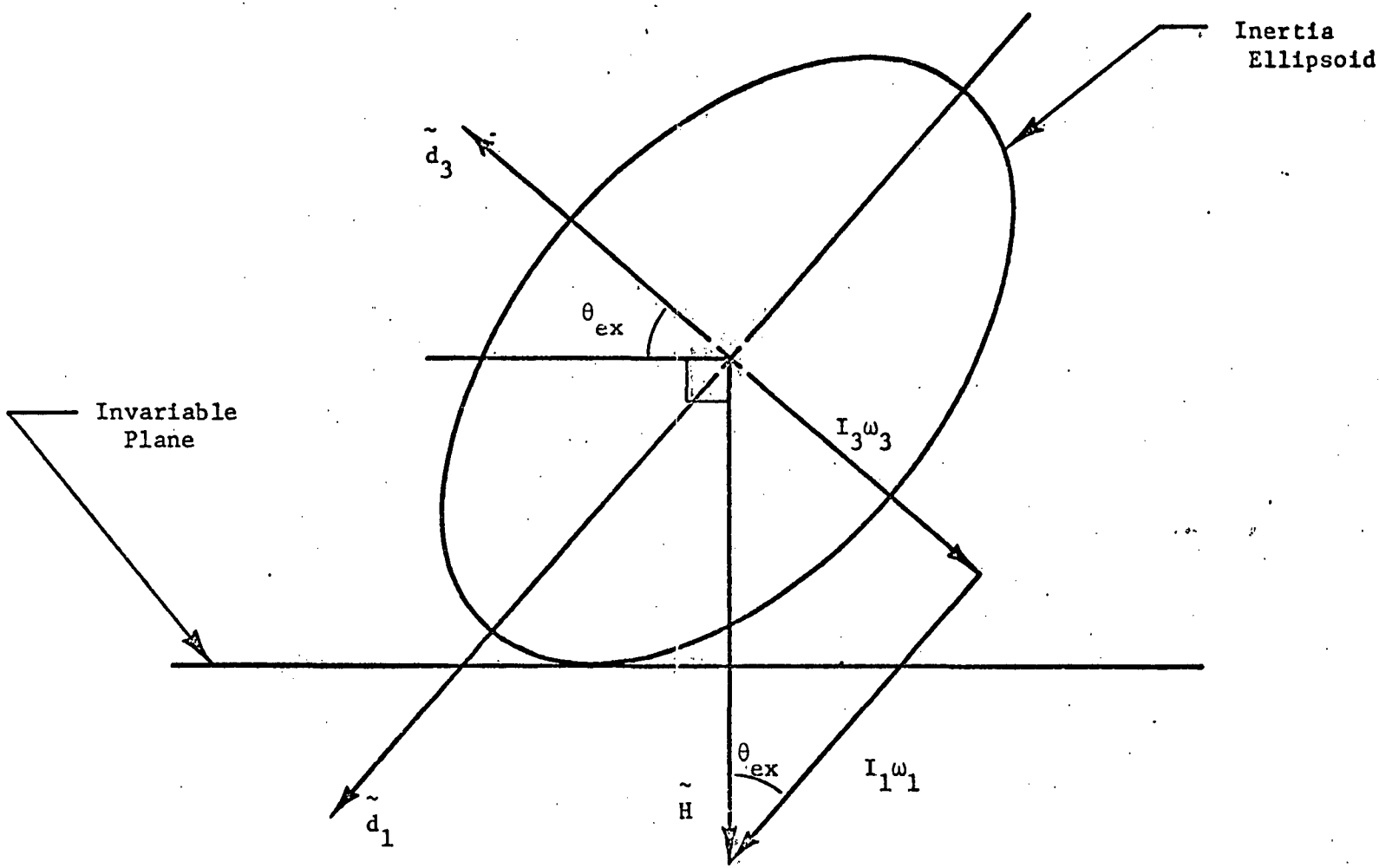

Figure 5. Extreme Position of $\tilde{d}_3$ Axis

The above relations take into account the fact that at this point in the motion

$$\left.\begin{aligned} 2T &= I_1\omega_1^2 + I_3\omega_3^2 \\ H^2 &= I_1^2\omega_1^2 + I_3^2\omega_3^2 \end{aligned}\right\} \omega_2 = 0$$

Further manipulation yields

$$\sin^2\theta_{ex} = \frac{I_3(2I_1T-H^2)}{H^2(I_1-I_3)} + \frac{I_3^2}{I_1H^2(I_1-I_3)}\{ I_3\omega_3^2(I_1-I_3) - (2I_1T-H^2) \}$$

Again, bearing in mind the particular energy and momentum conditions at this point, the final term in brackets equals zero. Therefore,

$$\sin^2\theta_{ex} = \frac{2I_1I_3}{H_2(I_1-I_3)}T - \frac{I_3}{I_1-I_3}$$

To provide as general an interpretation as possible, introduce the following terms:

$$I_{13} = \frac{I_1}{I_3}$$

$$I_{12} = \frac{I_1}{I_2}$$

$$T^* = \frac{T}{T_{max}}$$

where T_{max} is the maximum possible energy state for a given angular momentum. Thus, $T_{max} = H^2/2I_1$. Making the above substitutions, the bounds on the nutation angle reduce to the following forms:

a. Motion above the separatrix ($T > H^2/2I_2$)

$$\theta_{ua} = 90^\circ + \arcsin \sqrt{\frac{1-T^*}{1-T_{13}}}$$

$$\theta_{\ell a} = 90^\circ - \arcsin \sqrt{\frac{1-T^*}{1-I_{13}}}$$

b. Motion below the separatrix ($T < H^2/2I_2$)

$$\theta_{ub} = \arcsin \sqrt{\frac{T^*-I_{13}}{I_{12}-I_{13}}}$$

$$\theta_{\ell b} = \arcsin \sqrt{\frac{T^*-I_{13}}{1-I_{13}}}$$

At this stage, two relationships are to be noted:

1) The intermediate moment of inertia (contained in the term I_{12}) has no effect on the nutation angle range above the separatrix, and no effect on the lower limit of θ below the separatrix.

2) At the separatrix

$$T = \frac{H^2}{2I_2}$$

$$T^* = \frac{I_1}{I_2} = I_{12}$$

For a specific body having a minimum to maximum inertia ratio of one half ($I_{13} = 0.5$) the range of T^* is given by $0.5 \leq T^* \leq 1.0$. Figure 6 shows a plot of the bounds on θ vs T^*, assuming that $I_{12} = I_{13}$. Therefore, the first pair of equations holds for the entire range of T^*. This case corresponds to a thin rod, initially spinning about

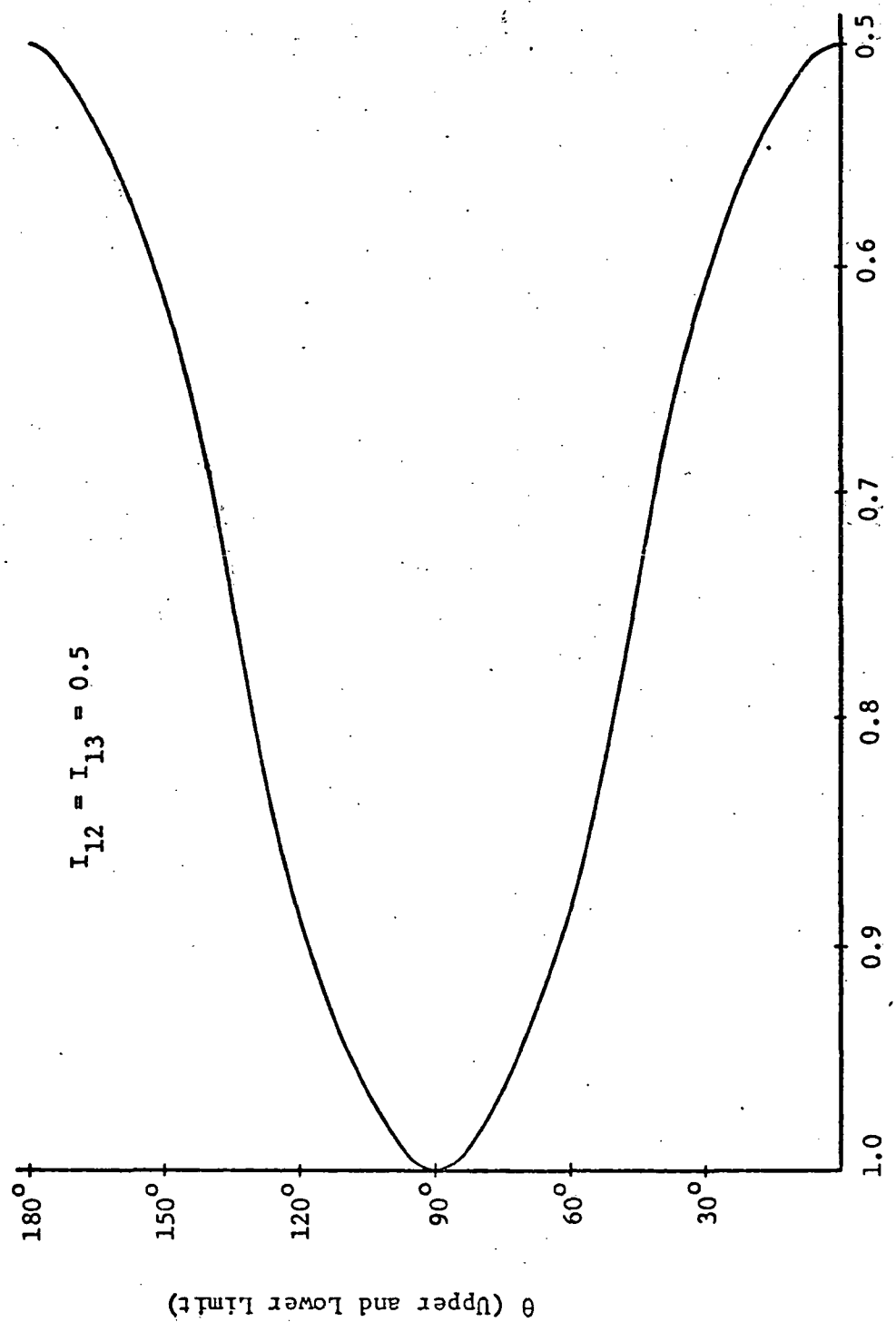

Figure 6. Bounds on θ for Symmetric Dissipative Body

its axis of minimum moment of inertia. As any transverse axis has the same (maximum) moment of inertia, the final nutation angle can take on any value between 0^o and 180^o. Figure 7 shows the bounds on θ for a body having the same I_{13}, but with an intermediate ratio, $I_{12} = 0.8$. This value for T* (T* = I_{12} = 0.8) can be seen as the critical point in the motion, as the bounds on θ divide into two regions: one ending in a final nutation angle of zero, the other ending in a final θ of 180^o, i.e., $\tilde{d}_3$ pointing in the opposite direction as $\tilde{\omega}$ and $\tilde{h}$.

Noting the continuity of the minimum values for θ at the transition point, the following relations can be written:

$$\theta_{\ell a} = 90^o - \arcsin \frac{1-T^*}{1-I_{13}}$$

$$= \arccos \frac{1-T^*}{1-I_{13}}$$

$$\theta_{\ell b} = \arcsin \frac{T^*-I_{13}}{1-I_{13}}$$

$$\cos^2\theta_{\ell a} = \frac{1-T^*}{1-I_{13}} \quad , \quad \sin^2\theta_{\ell b} = \frac{T^*-I_{13}}{1-I_{13}}$$

$$\cos^2\theta_{\ell a} + \sin^2\theta_{\ell b} = \frac{1-I_{13}}{1-I_{13}} = 1$$

$$\theta_{\ell a} = \theta_{\ell b}$$

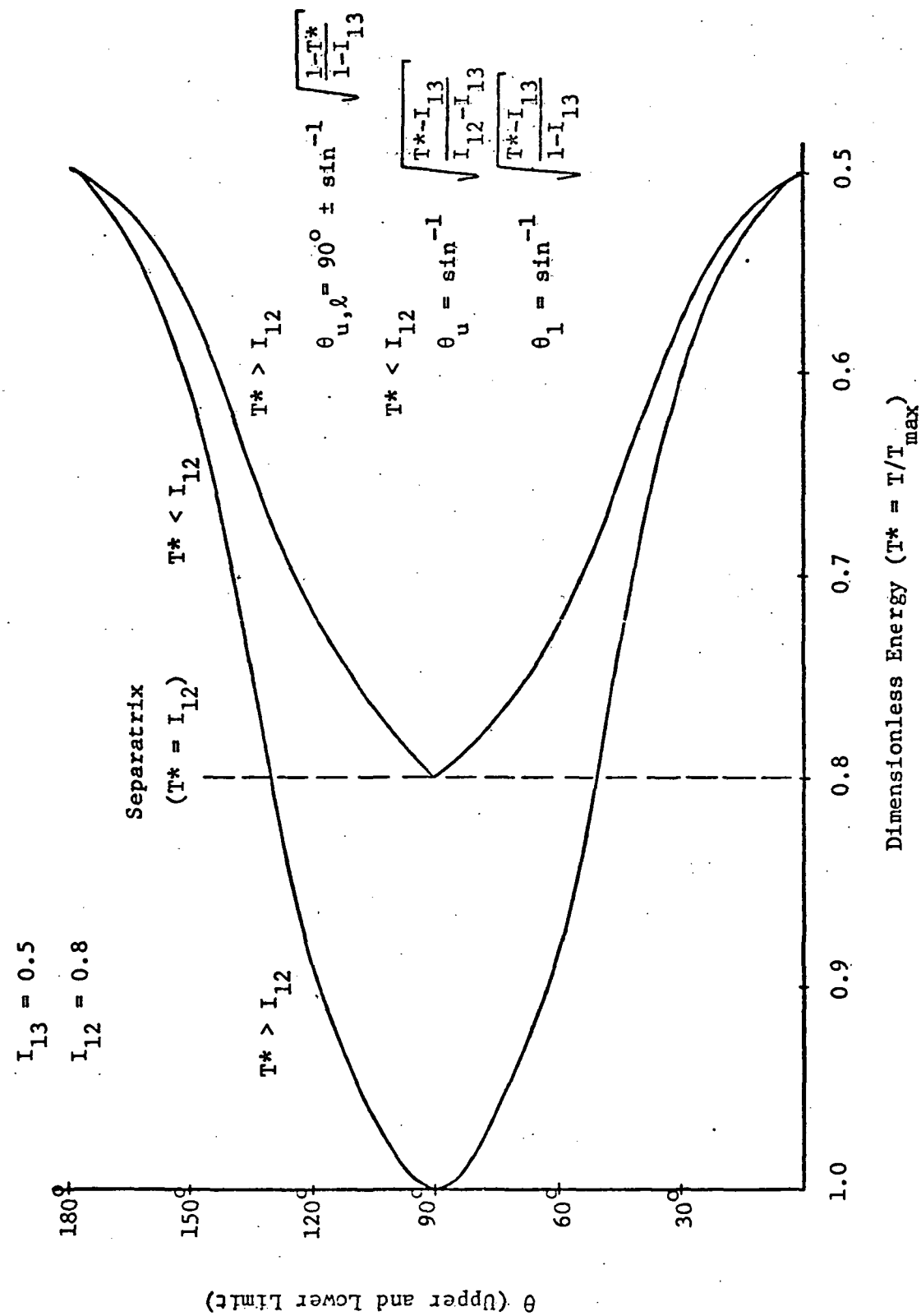

Figure 7. Bounds on θ for Non-Symmetric Dissipative Body

This is consistent with the earlier observation that I_{12} did not affect the bounds $\theta_{\ell b}$, θ_{ub}, and $\theta_{\ell a}$, as the value for I_{12} has no effect on these portions of the curve.

From the above description of tumbling motion it is apparent that the critical point in the motion is where the energy satisfies

$$T = H^2/2I_2 \quad .$$

At this point either the nutation angle or the sign of ω_3 identifies which direction the final spin vector will assume. As the nutation angle is rather difficult to measure, the sign of ω_3 will be used to determine the need for a control device. Assuming the control algorithm outlined in Figure 8, magnitudes of the three components of $\tilde{\omega}$, along with the sign of ω_3, must be known. Sensors are readily available for such application. Thus, it will be assumed that such equipment will be included in the satellite.

With the rotation vector $\tilde{\omega}$ known, real time calculations of the energy state and the dimensionless energy parameter T* can be made. Comparison of T* with the constant I_{12} then determines when the critical energy state has been reached, as $T^* = I_{12}$ at the critical point.

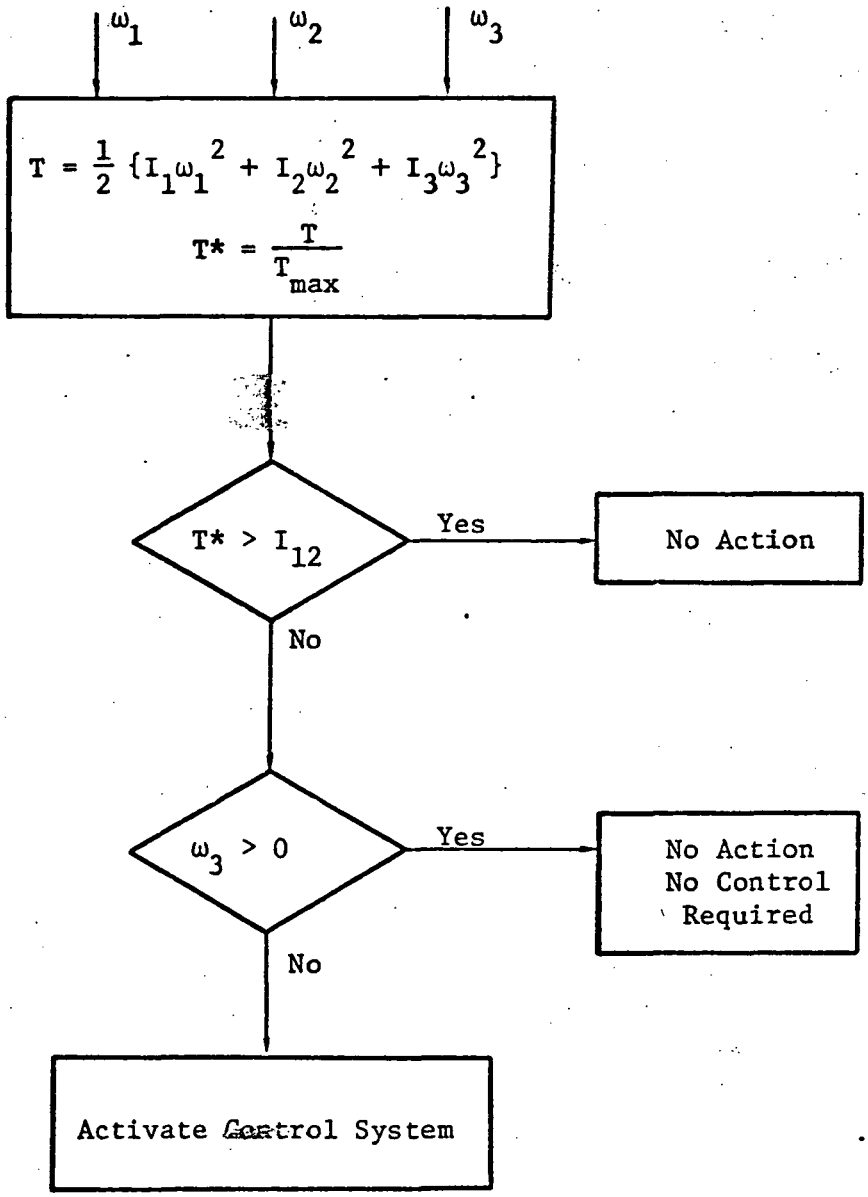

Figure 8. Algorithm for Elimination of Spin Ambiguity.

CONTROL SYSTEM ANALYSIS

Assuming that some control is required, three methods are discussed here. Moving masses in such a way as to lower the ratio I_{12} results in T* again being greater than I_{12}. Thus, the motion continues with $\tilde{\omega}$ lying above the separatrix level. When ω_3 becomes positive, the masses are returned to their original positions, and I_{12} is raised to its original value. While some energy is added in this process the net effect still leaves $\tilde{\omega}$ crossing the separatrix in the desired area. Starting an electric motor within the satellite increases the energy, and therefore T*, again allowing more time for $\tilde{\omega}$ to move around until ω_3 is positive. At this point, the motor is stopped, and again $\tilde{\omega}$ crosses the separatrix in the desired area. Both of the above systems are attractive in that they are completely internal in nature. Thus, the angular momentum vector remains unchanged, i.e., given the initial conditions, the final state is dictated. However, the size and orientation of the control elements must be such that sufficient change in I_{12} or T* must be generated to insure that $\tilde{\omega}$ does not cross the separatrix a second time before ω_3 becomes positive. Depending on the size of the satellite and the energy dissipation rates, this may require excessive size or volume requirements to effectively control the spin.

In these cases it may be necessary to go to an external torque to control the spin, i.e., reaction jets. These could be applied to increase the energy should the need arise, and decrease it again at the appropriate time. This, however, will result in some shifting of the final angular momentum vector. A final choice of a control system will depend on the individual situation.

For the first method suggested, motion of the masses could result in some loss of energy (see Appendix B). Thus, some criteria are required to verify that the change in I_{12} is sufficient to overcome any loss in energy. For the configuration shown in Figure 9,

$$I_{1B} = I_1 + A + 2mr^2$$

$$I_{2B} = I_2 + B + 2mR^2$$

$$I_{3B} = I_3 + C + 2m\ (R^2 + r^2)$$

where the subscript 'B' denotes before the weight shift. Similarly, with 'A' denoting after the weight shift,

$$I_{1A} = I_{1B} - 2mr^2$$

$$I_{2A} = I_{2B} + 2mr\ (2R + r)$$

$$I_{3A} = I_{3B} + 2mRr$$

From these, the following momentum and energy relationships can be written:

$$\tilde{h}_B = \omega_{1B} I_{1B} \tilde{i} + \omega_{2B} I_{2B} \tilde{j} + \omega_{3B} I_{3B} \tilde{k}$$

$$T_B = \frac{1}{2} \{I_{1B} \omega_{1B}^2 + I_{2B} \omega_{2B}^2 + I_{3B} \omega_{3B}^2\}$$

$$T_{maxB} = \frac{h_B^2}{2I_{1B}}$$

$$T^*_B = \frac{T_B}{T_{maxB}} = \frac{I_{1B}}{h_B^2} \{I_{1B} \omega_{1B}^2 + I_{2B} \omega_{2B}^2 + I_{3B} \omega_{3B}^2\}$$

$$\tilde{h}_A = \omega_{1A} I_{1A} \tilde{i} + \omega_{2A} I_{2A} \tilde{j} + \omega_{3A} I_{3A} \tilde{k}$$

$$T_A = \frac{1}{2} \{ I_{1A} \omega_{1A}^2 + I_{2A} \omega_{2A}^2 + I_{3A} \omega_{3A}^2 \}$$

$$T_{maxA} = \frac{h_A^2}{2 I_{1A}}$$

$$T^*_A = \frac{T_A}{T_{maxA}} = \frac{I_{1A}}{h_A^2} \{ I_{1A} \omega_{1A}^2 + I_{2A} \omega_{2A}^2 + I_{3A} \omega_{3A}^2 \}$$

The magnitudes of $\tilde{h}_A$ and $\tilde{h}_B$ must be equal. If the masses are assumed to move quickly with respect to the rotation rates of the satellite, the components of $\tilde{h}_A$ can be assumed to be equal to the components of $\tilde{h}_B$. These conditions yield:

$$\tilde{h}_A = \tilde{h}_B = \tilde{h}$$

$$\omega_{1A} = \frac{I_{1B}}{I_{1A}} \omega_{1B} \qquad\qquad I_{12B} = \frac{I_{1B}}{I_{2B}}$$

$$\omega_{2A} = \frac{I_{2B}}{I_{2A}} \omega_{2B}$$

$$\omega_{3A} = \frac{I_{3B}}{I_{3A}} \omega_{3B} \qquad\qquad I_{12A} = \frac{I_{1A}}{I_{2A}}$$

At the crossover point, $T^*_B = I_{12B}$.

$$I_{1B} \omega_{1B}^2 + I_{2B} \omega_{2B}^2 + I_{3B} \omega_{3B}^2 = \frac{h^2}{I_{2B}}$$

The desired result is for $T^*_A > I_{12A}$

$$\frac{I_{1A}}{h^2}\{I_{1A}\omega_{1A}^2 + I_{2A}\omega_{2A}^2 + I_{3A}\omega_{3A}^2\} > \frac{I_{1A}}{I_{2A}}$$

$$I_{1A}\omega_{1A}^2 + I_{2A}\omega_{2A}^2 + I_{3A}\omega_{3A}^2 > \frac{h^2}{I_{2A}}$$

Substitution of h^2 from the equation for T^*_B at the crossover point results in:

$$I_{1B}\omega_{1B}^2\left\{\frac{I_{1B}I_{2A}-I_{2B}I_{1A}}{I_{1A}I_{2A}}\right\} + I_{3B}\omega_{3B}^2\left\{\frac{I_{3B}I_{2A}-I_{2B}I_{3A}}{I_{3A}I_{2A}}\right\} > 0$$

To insure that this is true (thus $T^*_A > I_{12A}$),

$$I_{1B}I_{2A} - I_{2B}I_{1A} > 0$$

$$I_{3B}I_{2A} - I_{2B}I_{3A} > 0$$

Substituting for I_{1A}, I_{2A}, and I_{3A} yields:

$$I_{1B}(2R + r) + r\, I_{2B} > 0$$

$$I_{3B}(2R + r) - R\, I_{2B} > 0$$

The first condition is always satisfied. The second can be rewritten as:

$$2 + \frac{r}{R} > \frac{I_{2B}}{I_{3B}}$$

As $I_{2B} < I_{3B}$ (by definition of the problem), this condition is satisfied for any positive values for r and R. Thus, the motion of any masses in the configuration illustrated in Figure 9 will result in the motion subsequent to the weight shift being above the separatrix ($T^*_A > I_{12A}$).

Use of the momentum wheel, the second method proposed, is the simple addition of energy to the system. For the simulation case used, the motor was aligned with the $\bar{d}_1$ axis, to produce as large an effect as possible on the angular velocity vector $\tilde{\omega}$. The reasoning behind this choice is shown in Figure 10 where it can be seen that the easiest way to physically move $\tilde{\omega}$ above the separatrix is to increase ω_1. Thus, the control motor for the simulation was mounted accordingly.

The final method considered is the straight forward application of an external torque through the use of attitude control thrusters. As mentioned previously, this is probably the least desirable of the potential control methods, as it results in a shifting of the angular momentum vector in inertial space. However, it is a possible means of controlling the final spin by the simple addition of energy (positive torque) should $\tilde{\omega}$ cross the separatrix at the incorrect interval, and the reduction of energy (negative torque) when the desired state has been reached.

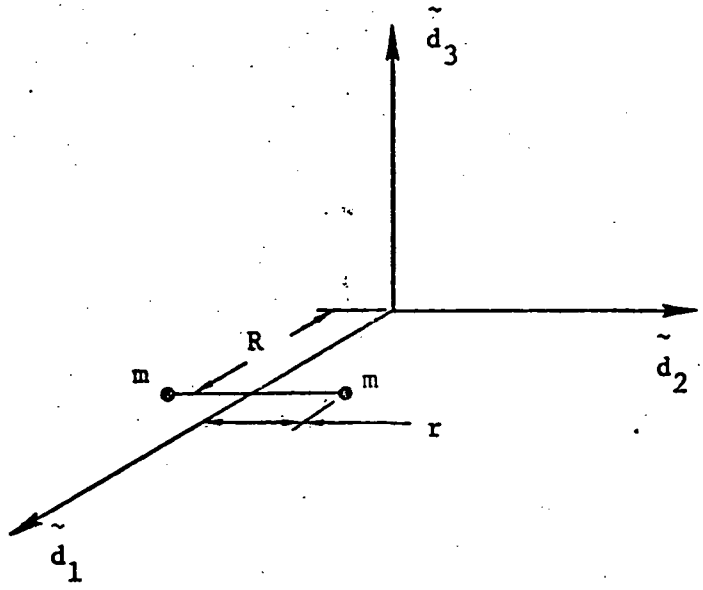

Figure 9. Simulated Control Mass Orientation

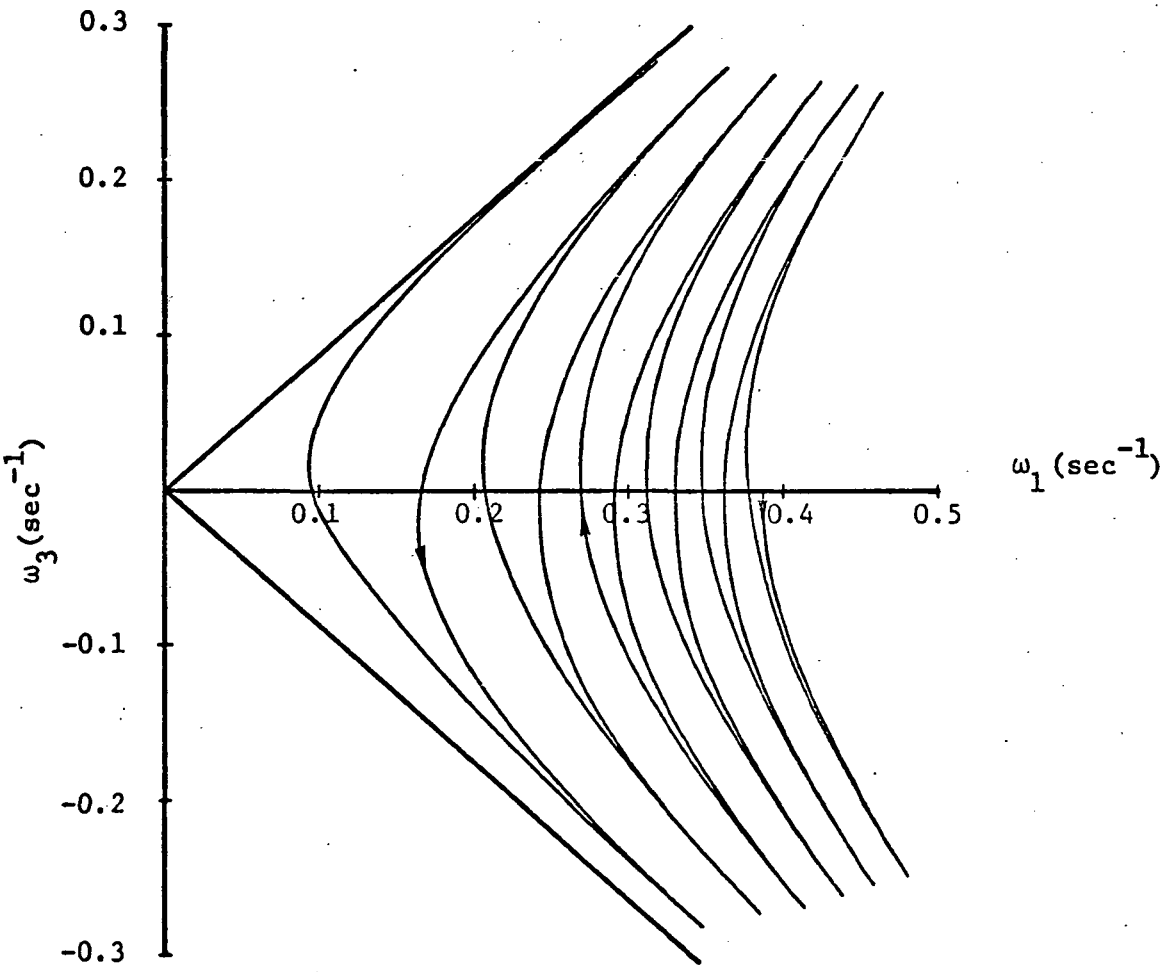

Figure 10. Projection of $\tilde{\omega}$ in $\tilde{d}_1$ - $\tilde{d}_3$ Plane.

SIMULATIONS AND RESULTS

The dynamic simulation used is very close to that used in Reference 4. This consists of a rigid satellite with a fluid ring damper mounted around the axis of maximum moment of inertia, in the plane of the transverse axes of inertia. Partially filling this ring with damping fluid results in some motion of the center of gravity of the satellite. Use of the characteristics for the partially filled damper with Euler's equations (for motion about a fixed point) results in some oscillation in the inertial angular momentum. Since the principal concern of this study is the relationship between the spacecraft orientation and the inertial angular momentum, two alternatives were considered for correcting this problem: (1) use of equations derived in Reference 14 for motion of a body with moving masses, and, (2) use of a fully filled fluid damper, eliminating the moving mass center. Use of the first method would involve considerably more computer time to handle the complex differential equations arising from the motion of the center of mass. This added time and effort would add little or no information concerning the point of interest here, control of the final spin vector. The second method, while seldom used in practical applications due to very low dissipation rates as steady spin is approached, does provide realistic energy dissipation in the region of interest, with the advantage of a simple, relatively accurate mathematical model. Thus, the second method was chosen and the equations of motion derived accordingly (See Appendix C). For the weight shift control method, these equations (before the weight shift) are:

$$\dot{\omega}_1 = \frac{\omega_2\omega_3(I_2 + A - I_3 - 2mr^2) - C\omega_2(\omega_3 + \dot{\alpha})}{I_1 + A + 2mr^2}$$

$$\dot{\omega}_2 = \frac{\omega_1\omega_3(I_3 + 2mR^2 - I_1 - A) + C\omega_1(\omega_3 + \dot{\alpha})}{I_2 + A + 2\,mR^2}$$

$$\dot{\omega}_3 = \frac{\omega_1\omega_2(I_1+2m(r^2-R^2)-I_2) + \frac{0.0395\ CR_{ad}{}^P}{SR_n{}^{1/4}}\left(\frac{|\dot{\alpha}|}{\dot{\alpha}}\right)\dot{\alpha}^2}{I_3 + 2m\,(R^2 + r^2)}$$

$$\ddot{\alpha} = \frac{-0.0395\ R_{ad}{}^P}{SR_n{}^{1/4}}\left(\frac{|\dot{\alpha}|}{\dot{\alpha}}\right)\dot{\alpha}^2 - \dot{\omega}_3$$

Appropriate changes in the moments of inertia and application of the same manipulations provide similar equations for the motion after the masses have been shifted. These equations are then solved in the simulation diagrammed in Figure 11. For all the simulations, a fourth order Runge-Kutta method is used to solve the differential equations, using a time step of 0.25 sec. Several time steps were tried, but 0.25 sec. gives the best compromise between desirable accuracy and reasonable simulation time for a given amount of computer time.

All equations are solved in the body fixed coordinate system. To provide the nutation angle θ and to verify the accuracy of the entire simulation, Euler's angles (ψ,ϕ,θ) are calculated using the following equations.[15]

$$\dot{\psi} = \frac{1}{\sin\theta}\ (\omega_1 \sin\phi + \omega_2 \cos\phi)$$

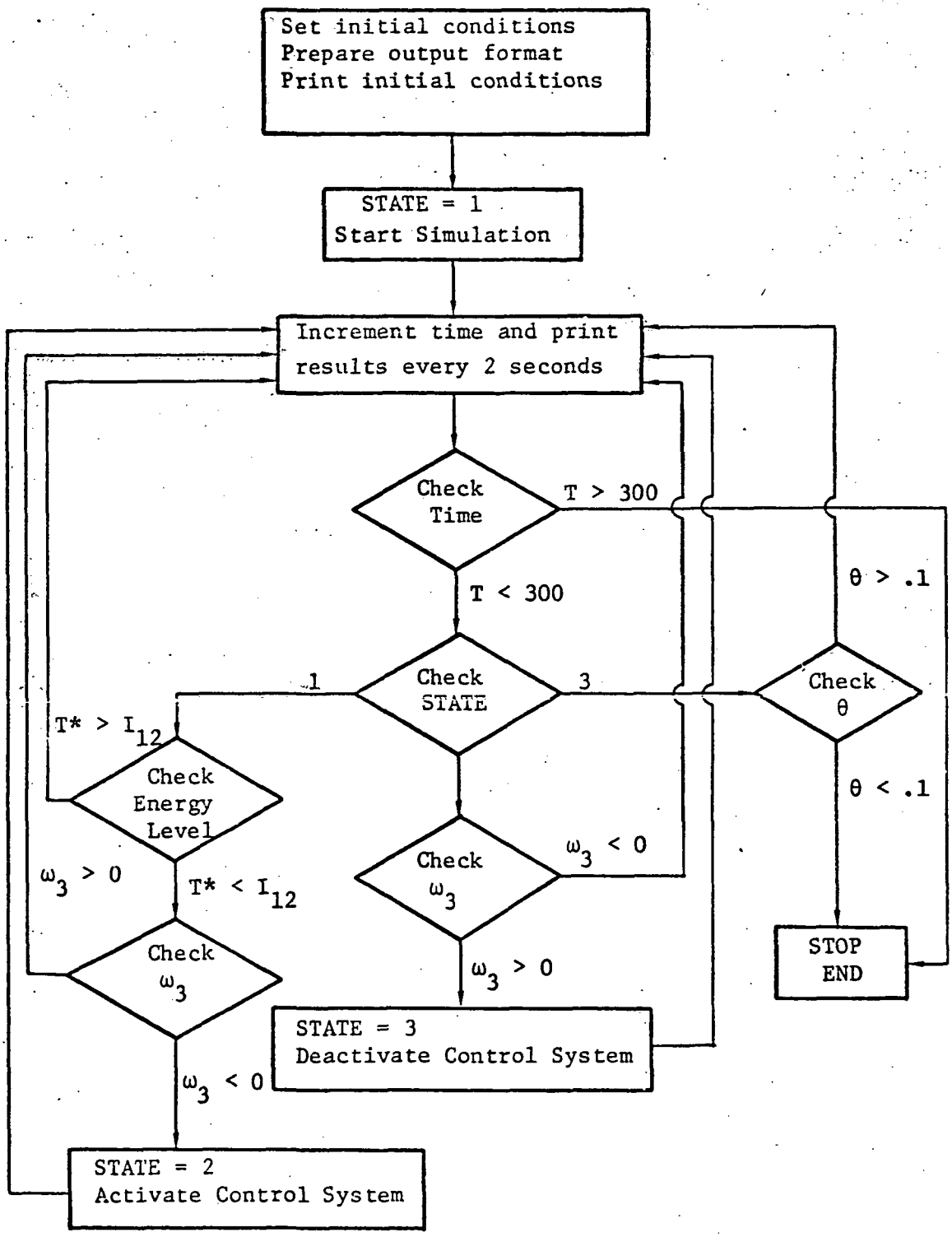

Figure 11. Flow Chart for Computer Simulation.

$$\dot{\phi} = \omega_3 - \frac{\cos\theta}{\sin\theta}(\omega_1 \sin\phi + \omega_2 \cos\phi)$$

$$\dot{\theta} = \omega_1 \cos\theta - \omega_2 \sin\phi$$

again with a fourth order Runge Kutta method. The values for Euler's angles are then used to transform the angular momentum from the body fixed to inertial co-ordinate systems. As this should remain constant for the first two control systems, it provides an easy check on the validity of the equations and the adequacy of the time step.

The spacecraft modeled is the vehicle presented in Reference 4. The appropriate physical properties are:

$$I_1 = 1785 \text{ ft-lb-sec}^2 \quad (2380 \text{ kg - m}^2$$

$$I_2 = 5190 \text{ ft-lb-sec}^2 \quad (6940 \text{ kg - m}^2)$$

$$I_3 = 6920 \text{ ft-lb-sec}^2 \quad (9250 \text{ kg - m}^2)$$

For the fluid damper the following figures apply:

$$\rho = 1.27 \times 10^{-3} \frac{\text{lb-sec}^2}{\text{in}^4} \quad (1.36 \times 10^4 \text{ kg/m}^3)$$

$$v = 1.8 \times 10^{-4} \text{ in}^2/\text{sec} \quad (1.16 \times 10^{-7} \text{m}^2/\text{sec})$$

} mercury as viscous fluid

$$R_{ad} = 4.35 \text{ ft.} \quad (1.33 \text{ m})$$

$$D = 0.13 \text{ ft.} \quad (0.0398 \text{ m})$$

For the control masses, the following values were chosen:

$$R = 1 \text{ ft.} \quad (0.30 \text{ m})$$

$$r = 3 \text{ ft.} \quad (0.91 \text{ m})$$

$m = 5$ lb. (2.26 kg)

It should be noted that simulations were run with smaller lengths and lighter masses. However, these proved insufficient for having the desired effect. With the above figures, the parameters I_{12} and I_{13} take on the values 0.402 and 0.289, respectively. Figure 12 shows the theoretical limits on the bounds on θ for this particular body. Figure 13 shows the results of the computer simulation for the angle θ. This case considers an angular momentum equivalent to an initial spin rate of ~ 10 rpm. The initial conditions are chosen such that the satellites energy state is relatively near the separatrix, yet far enough away to allow observation of several cycles before the critical point is reached. It should also be noted that initially the fluid slug has a body relative velocity of zero. Figures 13 and 14 show the nutation angle, energy state, ω_3, and dissipation rate for the first simulation. As can be seen from these figures, no control is required for this case, as θ is oscillating towards the final limit of 0^o, and ω_3 is oscillating towards a final positive value. These calculations are based on the empirical friction coefficient $f = 0.316/R_n^{1/4}$ for the fluid damper. Changing this coefficient by 5% has the effect of reversing the final outcome (see Figures 15 and 16). Thus, any attempt to predict the crossover point and control the final spin orientation by alteration of the initial conditions would require knowledge of the energy dissipation rate, to within at least 5%. Alternatively, Figure 17 shows this same second case with the moving masses incorporated into the system. As the energy reaches the separatrix level initially, θ is greater

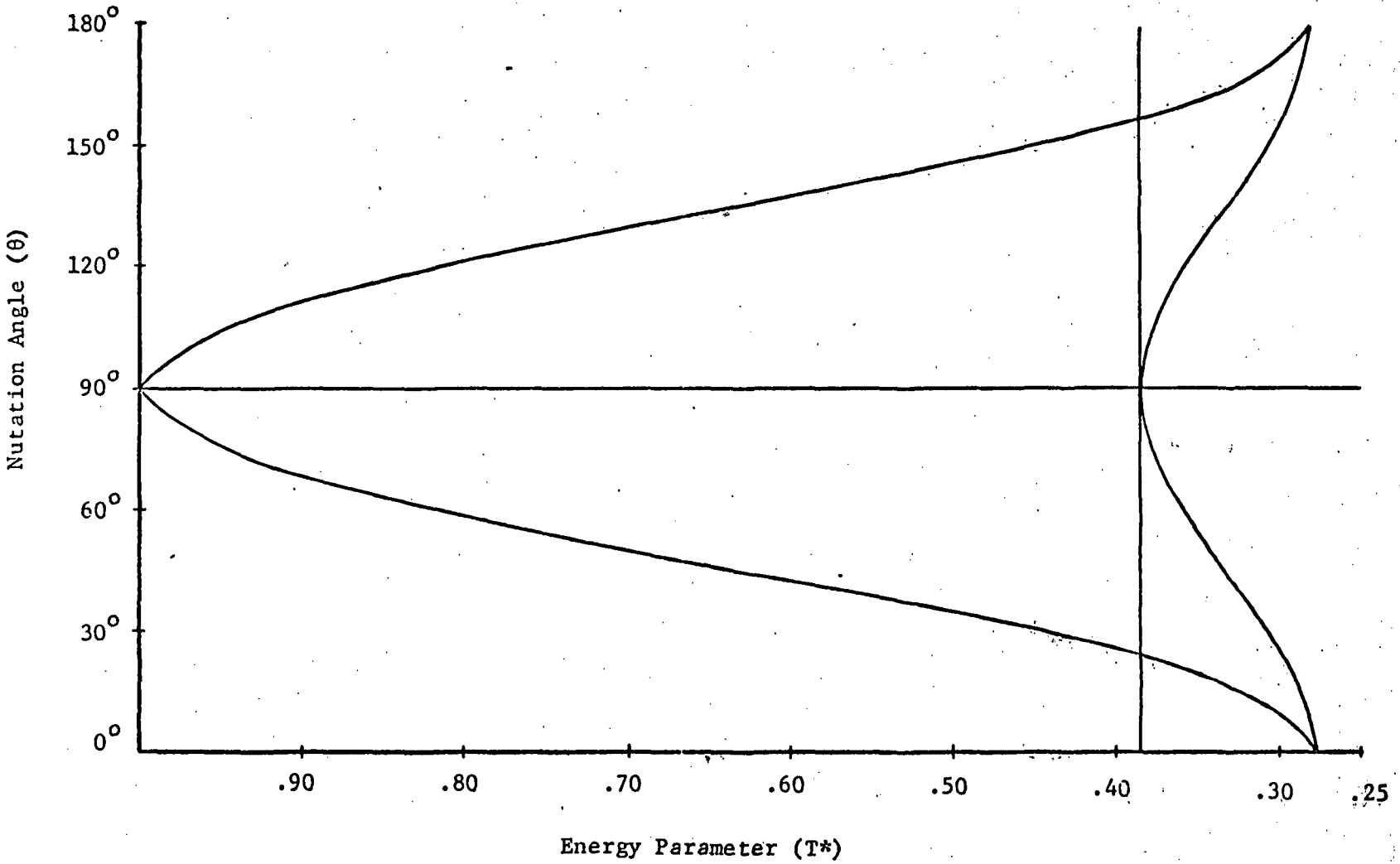

Figure 12. Bounds on θ for Simulation Case

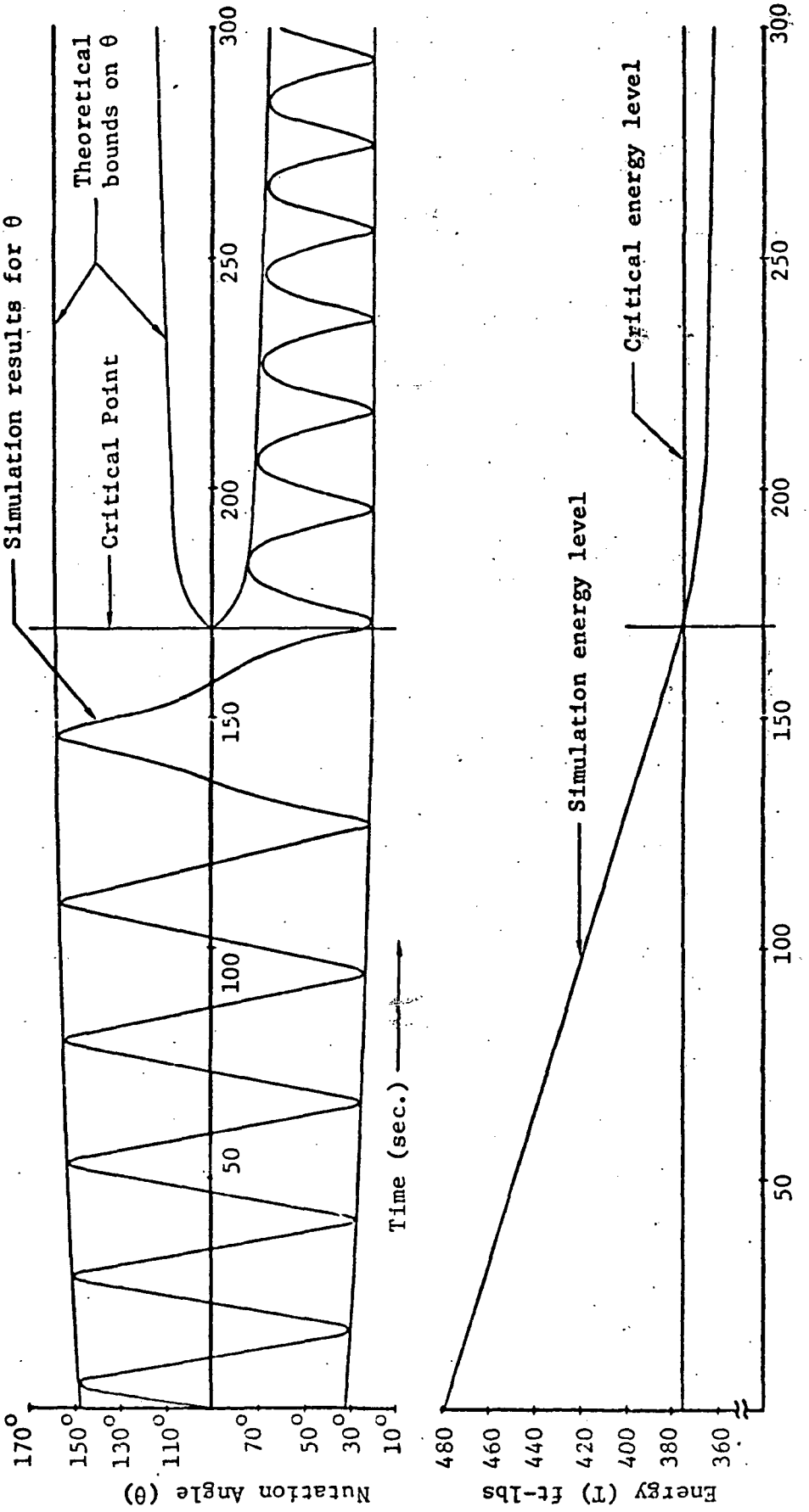

Figure 13. Nutation Angle and Energy for Desired Result.

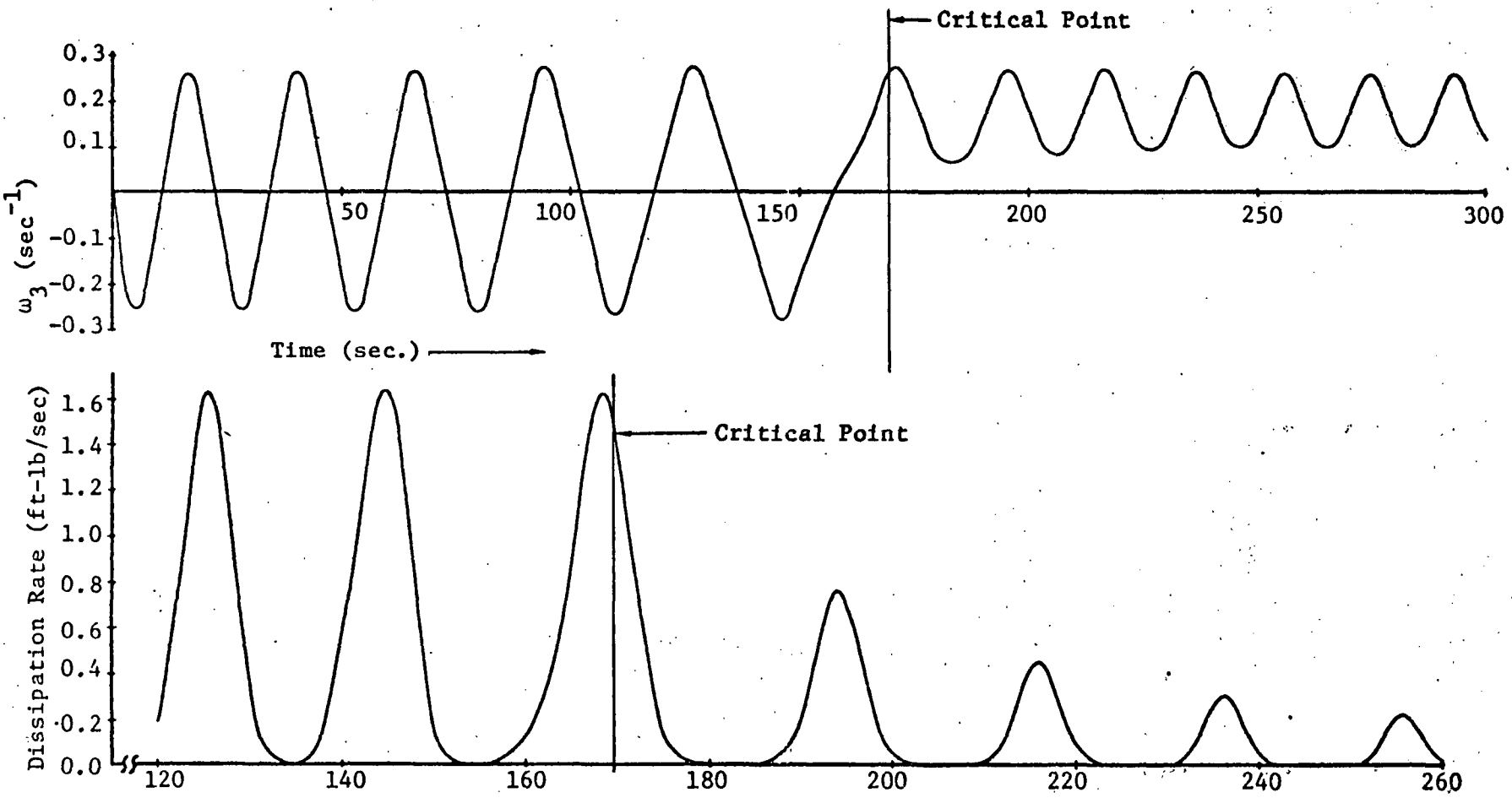

Figure 14. Dissipation Rate and ω_3 for Desired Result.

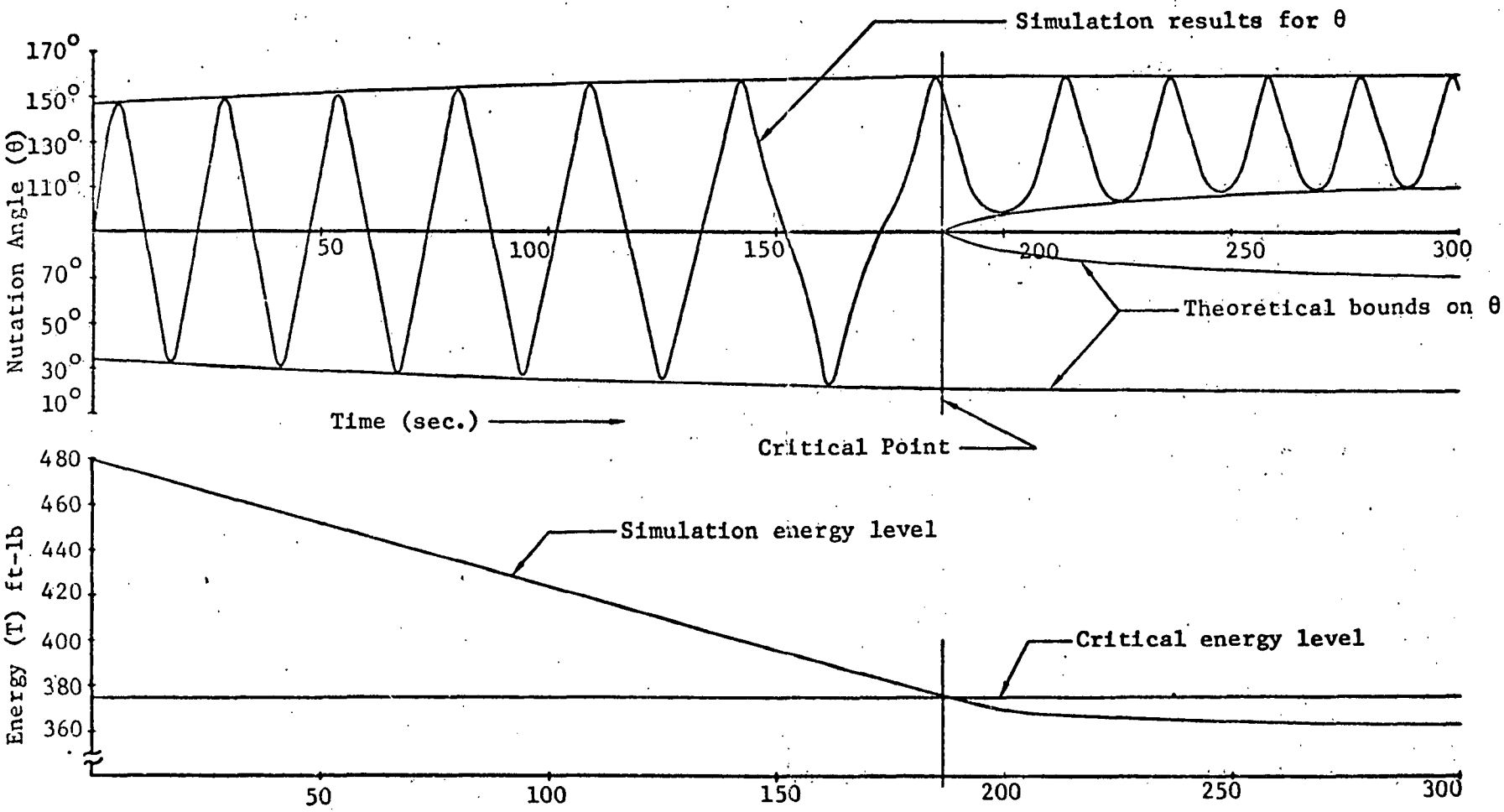

Figure 15. Nutation Angle and Energy for Incorrect Result.

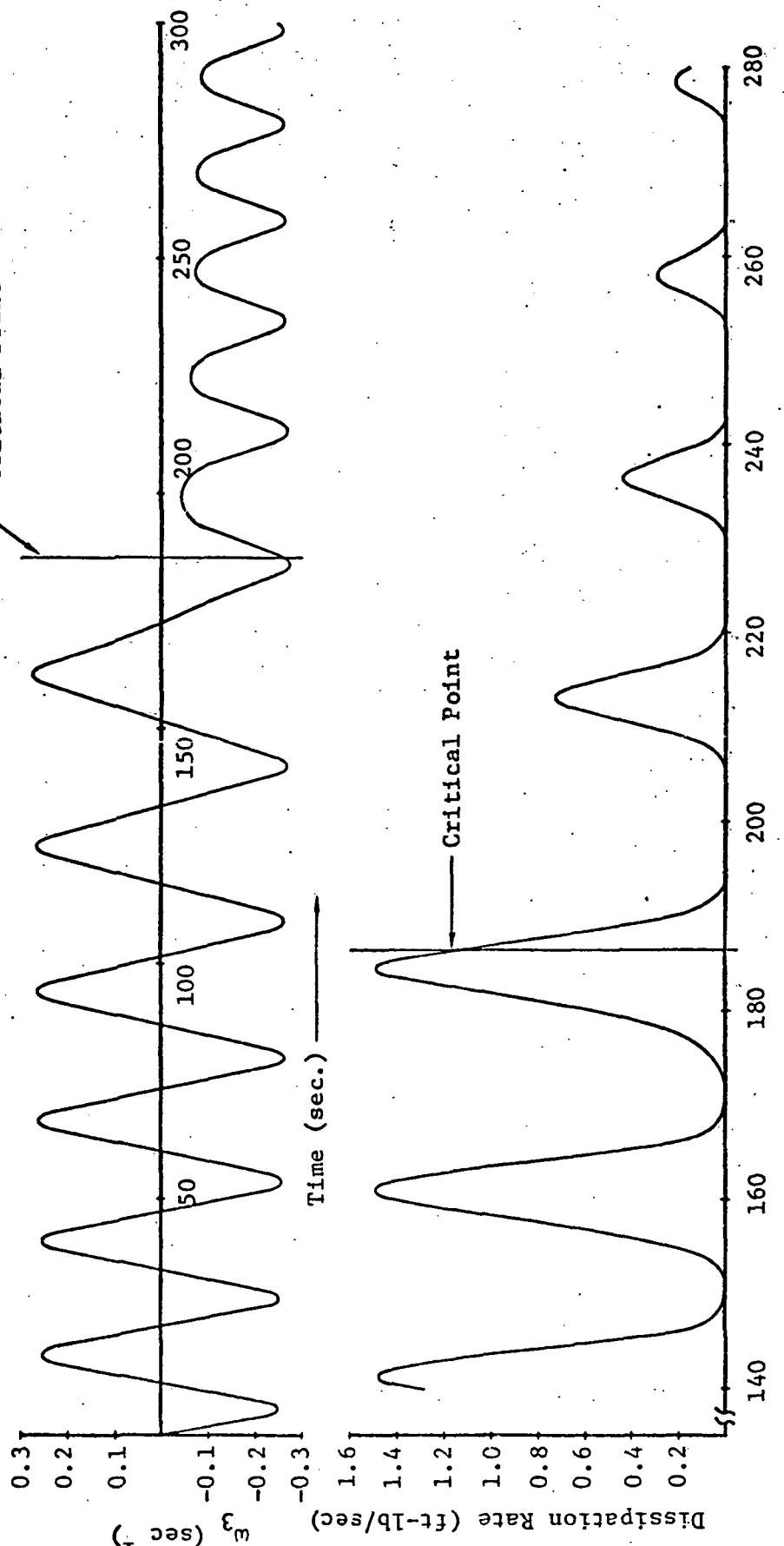

Figure 16. Dissipation Rate and ω_3 for Incorrect Result.

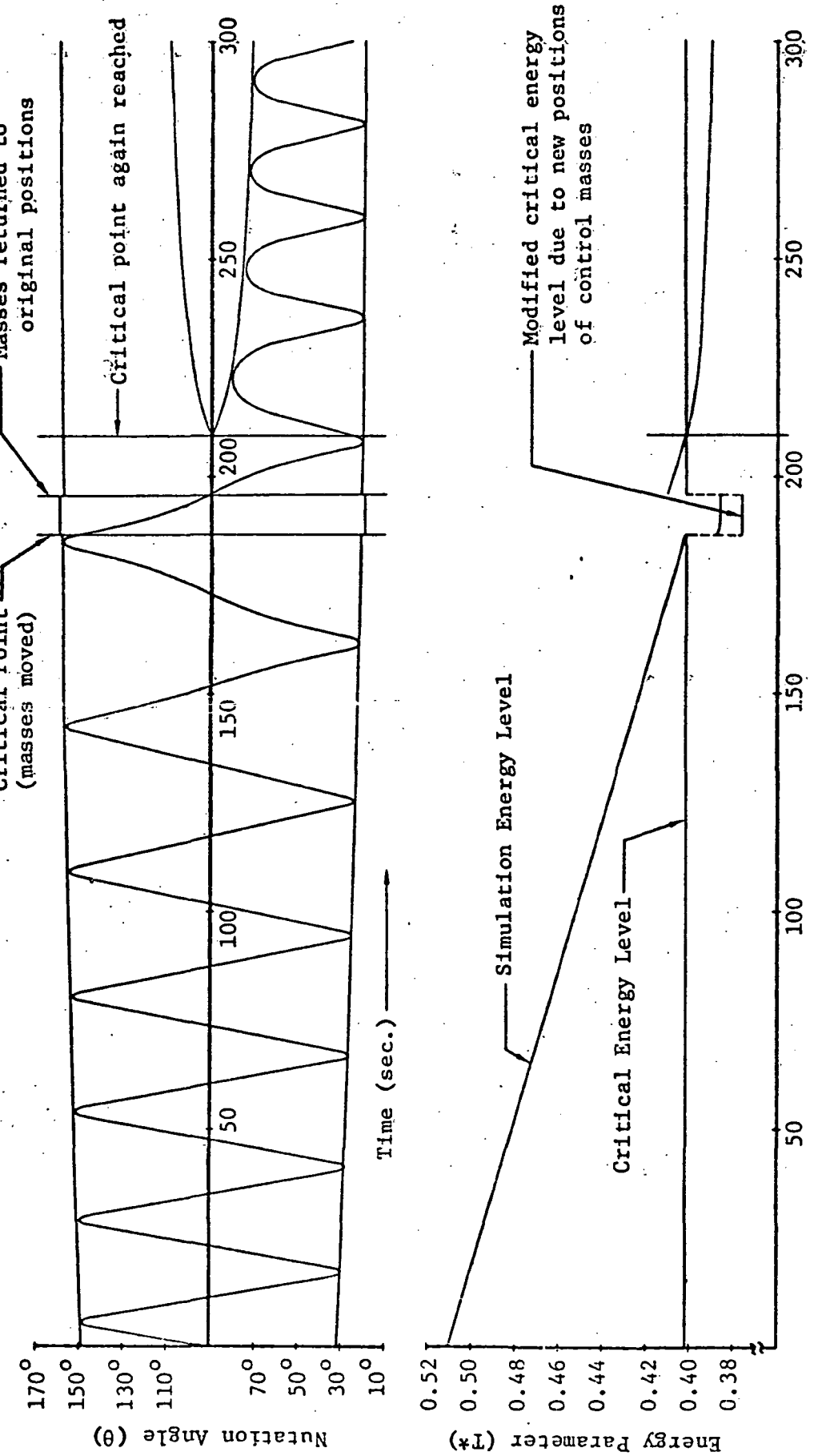

Figure 17. Nutation Angle and Energy Parameter for Moving Mass Control Method.

than 90°, therefore, it would oscillate towards the final value of 180°. Movement of the masses at this point results in the lowering of the ratio I_{12}, and therefore the critical energy level, allowing θ to oscillate below 90°. At this point, the masses are returned to their original positions I_{12} returns to its original value. The energy added by the movement of the masses is quickly dissipated, and the critical energy is again reached, with θ now oscillating towards 0°.

Using the electric motor control method and the initial conditions used to obtain Figures 15 and 16, the simulation produced the results shown in Figure 18. Rotor characteristics were taken as

$$I_{1R} = 0.05 \text{ ft-lb-sec}^2 \ (0.067 \text{ kg - m}^2)$$

$$I_{2R} = I_{3R} = 0.025 \text{ ft-lb-sec}^2 \ (0.034 \text{ kg m}^2)$$

$$h_R = 7.5 \text{ ft-lb-sec} \ (10.0 \ \frac{\text{kg - m}^2}{\text{sec}})$$

these being the characteristics of a large, commercially available momentum wheel. Three such wheels were required to produce the desired results. Figure 18 shows the energy state of the satellite, with addition of the rotor energy an obvious platform in the energy level as the critical state is reached with $\theta > 90^{\circ}$. Shutting off the motors as θ reaches 90° again allows θ to oscillate toward a final value of 0°.

Using attitude control thrusters, assuming a thrust of 5 lbs. for 3 seconds at a radius of 6 ft. produces the results shown in Figure 19. Again, the activation of the control system results in an increase in the energy, allowing θ to again return to the desired region ($\theta < 90^{\circ}$). Theoretical limits on θ are not given for this case after the application of the control torque, as the theory gives

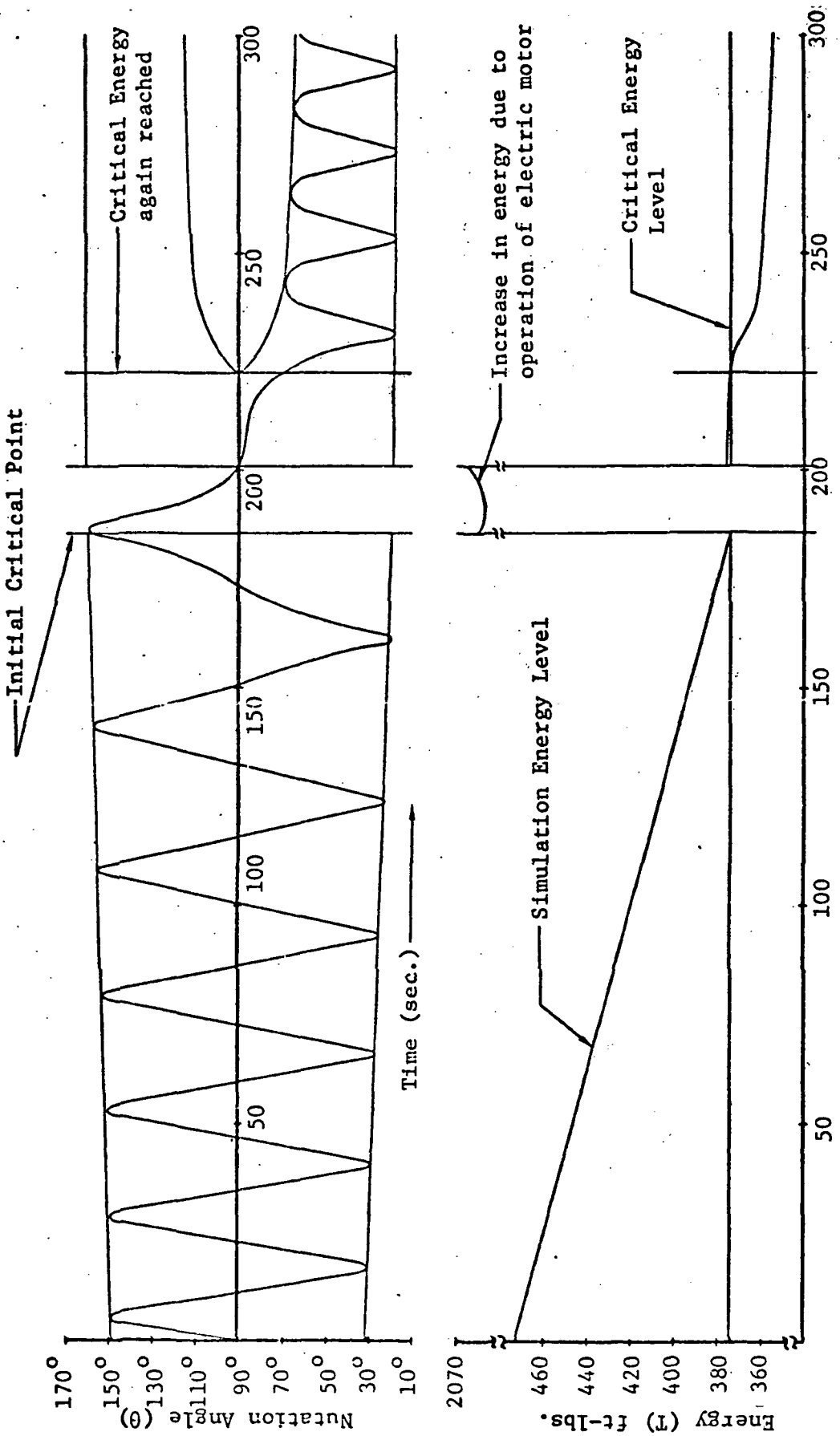

Figure 18. Nutation Angle and Energy State for Electric Motor Control Method.

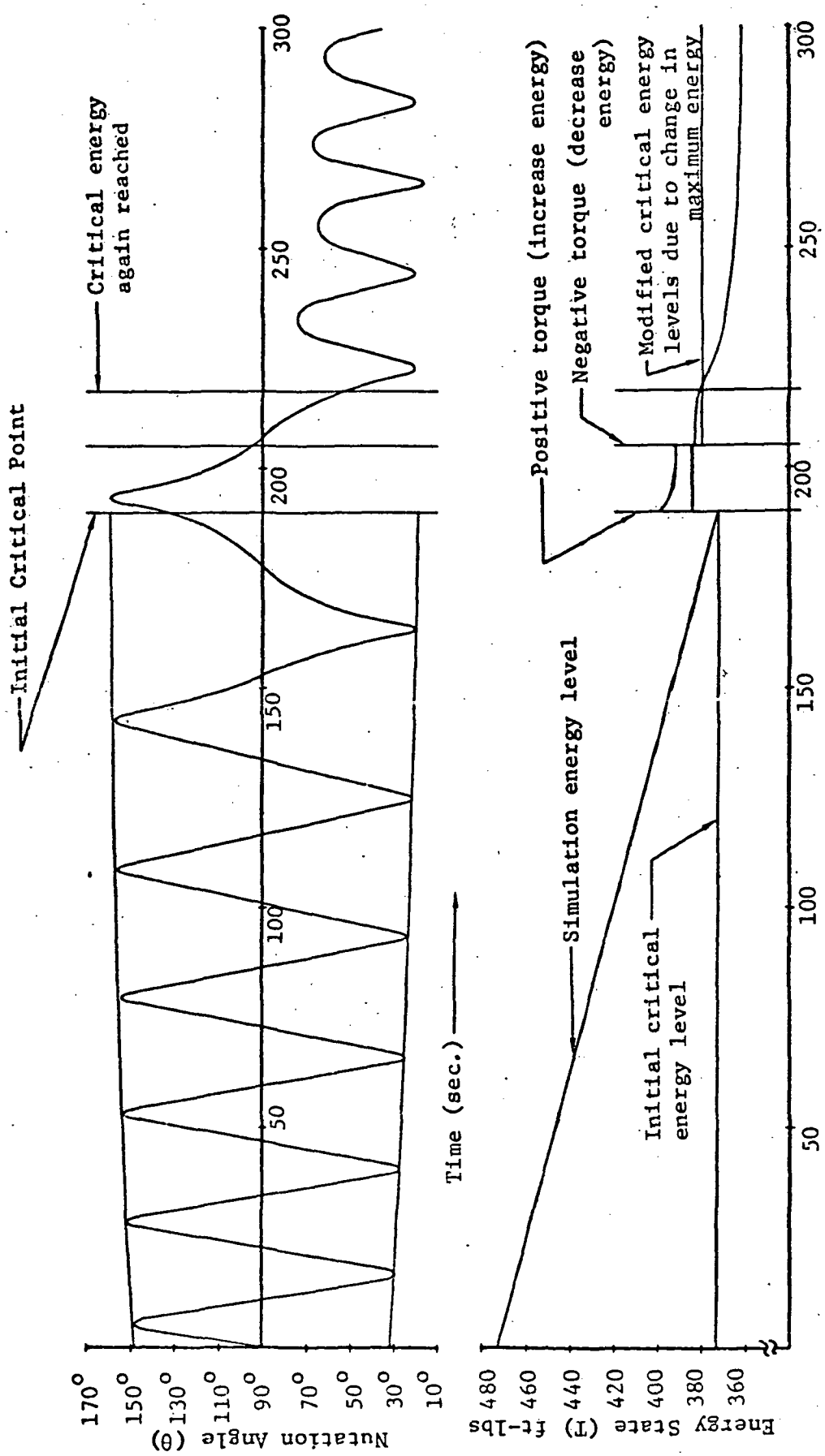

Figure 19. Nutation Angle and Energy State for Reaction Jet Control Method.

θ as the angle between $\tilde{d}_3$ and the angular momentum vector. In the preceding cases this coincided with the z-axis of inertial space. The external torque results in a deviation of the direction of the angular momentum vector of approximately 3.4° while θ is still being measured from the z-axis. This accounts for the irregular nature of the oscillations after the application of the control torques. Application of the external torque also results in a change in the magnitude of the angular momentum vector of approximately 1%.

CONCLUSIONS

The analytical expressions developed for the nutation angle θ, coupled with the simulation results coinciding with the predictions, appear to verify that a tumbling body exhibits two distinct types of motion. For an energy state greater than $h^2/2I_2$ (where $I_1 < I_2 < I_3$) the nutation angle oscillates symmetrically about 90°, while ω_3 oscillates through positive and negative values. At the point where the energy equals $h^2/2I_2$ motion is transformed, with θ and ω_3 still oscillatory functions; however θ now oscillates toward either 0° or 180°, while ω_3 remains either a positive or negative function, oscillating towards the final stable value in either the positive or negative sense. Control over this final orientation can be most easily accomplished at the critical point $T = h^2/2I_2$ by varying either the moments of inertia, the energy state, or both. The work presented here verifies that the motion can be controlled by the use of either moving masses, electric motors, or thrusters, along with minimal sensing equipment. The most attractive method appears to be the moveable masses, as relatively large electric motors were required to handle the sample case presented. Thrusters, while originally felt undesirable, may, with further work, prove to have one large advantage. This lies in flexibility of control. While either the mass or the motors would have to be sized for worst case conditions, it may be possible to derive an optimum thrust for any particular case, thus, minimizing both the deviation in the angular momentum vector and the mass needed to effectively control the motion.

REFERENCES

1. Thomson, W. T. and Reiter, G. S., "Attitude Drift of Space Vehicles," Journal of the Astro. Sciences, No. 7, 1960, pp. 29-34.

2. Bracewell, R. N. and Garriott, O. K., "Rotation of Artificial Earth Satellites," Nature, 182, 20 September 1958, pp. 760-762.

3. . . . "Final Report on a Study of Automated Rendezvous and Docking for ATS-V Despin," Space Division, North American Rockwell, Contract NASW-2136, February 1971.

4. Kaplan, M. H. and Beck, N. M., "Attitude Dynamics and Control of Apogee Motor Assembly with Paired Satellites," Journal of Spacecraft and Rockets, No. 6, Vol. 9, 1972, pp. 410-415.

5. Likins, P. W. and Bouvier, H. K., "Attitude Control of Nonrigid Spacecraft," Astronautics and Aeronautics, May 1971, pp. 64-71.

6. Vigneron, R. F., "Motion of Freely Spinning Gyrostat Satellites with Energy Dissipation," Astronautica Acta, Vol. 16, 1971, pp. 373-380.

7. Meirovitch, L. and Nelson, H. D., "On the High-Spin Motion of a Satellite Containing Elastic Parts," Journal of Spacecraft and Rockets, No. 11, Vol. 5, 1966, pp. 1597-1602.

8. Kuebler, M. E., "Gyroscopic Motion of an Unsymmetrical Satellite under no External Forces," NASA Tech. Note D-596, July 1960.

9. Likins, P. W., "Effects of Energy Dissipation on the Free Body Motions of Spacecraft," Jet Propulsion Laboratory Tech. Rept. 32-860, July 1966.

10. Hopper, F. W., "Active Precession Control for Spin Stabilized Space Vehicles," AIAA Paper #71-952, presented at AIAA Guid., Control and Flight Mechanics Conference, Hofstra University, Hempstead, New York, 16-18 August 1971.

11. Kane, T. P. and Scher, M. P., "A Method of Active Attitude Control Based on Energy Considerations," Journal of Spacecraft and Rockets, No. 5, Vol. 6, 1969, pp. 633-636.

12. Alper, J. R., "Analysis of Pendulum Damper for Satellite Wobble Damping," Journal of Spacecraft and Rockets, No. 1, Vol. 2, 1964, pp. 50-54.

13. Synge, J. L. and Griffith, B. W., Principles of Mechanics, McGraw Hill Book Company, Inc., 1959, Chapters 13-14.

14. Grubin, C., "Dynamics of a Vehicle Containing Moving Parts," Journal of Applied Mechanics, September, 1962, pp. 486-488.

15. Thomson, W. T., Introduction to Space Dynamics, John Wiley and Sons, 1961, Chapter 3.

APPENDIX A

Definition of extreme values for θ

$$\sin^2\theta = \frac{\omega_1^2 I_1^2 + \omega_2^2 I_2^2}{h^2}$$

$$\theta = \arcsin \frac{1}{h}\sqrt{\omega_1^2 I_1^2 + \omega_2^2 I_2^2}$$

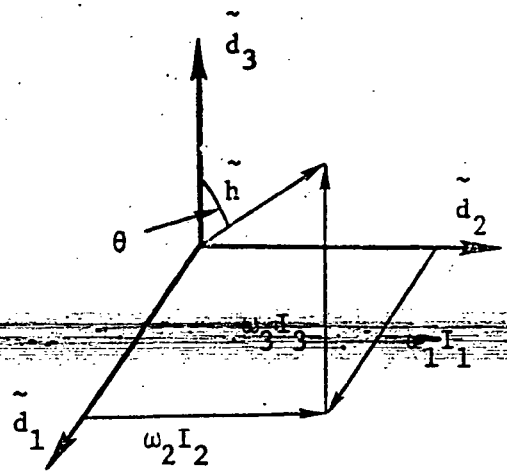

Orientation of $\tilde{h}$ in Body Fixed Coordinates

Figure A-1

$$\frac{d\theta}{dt} = \frac{\partial\theta}{\partial\omega_1}\frac{d\omega_1}{dt} + \frac{\partial\theta}{\partial\omega_2}\frac{d\omega_2}{dt}$$

$$= \frac{1}{\sqrt{1 - \frac{\omega_1^2 I_1^2 + \omega_2^2 I_2^2}{h^2}}} \cdot \frac{\omega_1 I_1^2}{h\sqrt{\omega_1^2 I_1^2 + \omega_2^2 I_2^2}}\frac{d\omega_1}{dt}$$

$$+ \frac{1}{\sqrt{1 - \frac{\omega_1^2 I_1^2 + \omega_2^2 I_2^2}{h^2}}} \cdot \frac{\omega_2 I_2^2}{h\sqrt{\omega_1^2 I_1^2 + \omega_2^2 I_2^2}}\frac{d\omega_2}{dt}$$

$$= \frac{1}{\omega_3 I_3\sqrt{\omega_1^2 I_1^2 + \omega_2^2 I_2^2}}\left\{\omega_1 I_1^2\frac{d\omega_1}{dt} + \omega_2 I_2^2\frac{d\omega_2}{dt}\right\}$$

For θ to be an extreme, $\frac{d\theta}{dt} = 0$.

with[15]
$$\omega_1 = \sqrt{\frac{h^2 - 2I_1T}{I_3(I_3-I_1)}} \quad dn\{(t-t_o)\sqrt{\frac{(2I_3T - h^2)(I_2 - I_1)}{I_1I_2I_3}}\}$$

$$\omega_2 = \sqrt{\frac{2I_3T - h^2}{I_2(I_3 - I_2)}} \quad sn\{(t-t_o)\sqrt{\frac{(2I_3T - h^2)(I_2 - I_1)}{I_1I_2I_3}}\}$$

$$\frac{d\omega_2}{dt} = 0 \quad \text{where } \omega_1 = 0$$

$$\frac{d\omega_1}{dt} = 0 \quad \text{where } \omega_2 = 0$$

Extreme values of θ coincide to points where either ω_1 or ω_2 equals zero.

APPENDIX B

Loss of energy through mass motion

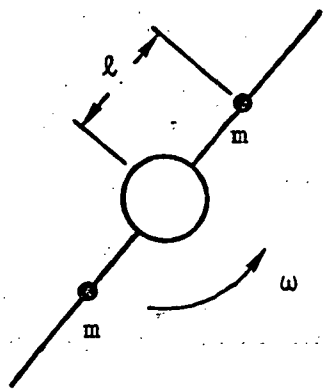

Consider a simply rotating body as illustrated with moment of inertia I. The two masses at distance ℓ from center result in a total $I_T = I + 2m\ell^2$

Therefore, the momentum and energy equations are

$$h = \omega(I + 2m\ell^2)$$

$$T = \frac{1}{2}(I + 2m\ell^2)\omega^2$$

Allowing the masses to move out to a length 2ℓ, the moment of inertia, momentum, and energy become:

$$I_T = I + 8m\ell^2$$

$$h = \omega_f (I + 8m\ell^2)$$

$$T_f = \frac{1}{2}(I + 8m\ell^2)\ \omega_f^2$$

where ω_f = final rotation vector. To maintain angular momentum,

$$\omega_f = \left(\frac{I + 2m\ell^2}{I + 8m\ell^2}\right)\ \omega$$

$$T_f = \frac{1}{2}\left(\frac{I + 2m\ell^2}{I + 8m\ell^2}\right)(I + 2m\ell^2)\ \omega^2$$

$$T_f = \left(\frac{I + 2m\ell^2}{I + 8m\ell^2}\right)\ T$$

$$T_f < T.$$

APPENDIX C

Derivation of equations of motion[4]

$$h_1 = \omega_1(I_1 + A + 2mr^2)$$

$$h_2 = \omega_2(I_2 + A + 2mR^2)$$

$$h_3 = \omega_3(I_3 + 2m\ (r^2 + R^2)) + C(\omega_3 + \dot{\alpha})$$

$$\dot{h}_1 = \dot{\omega}_1(I_1 + A + 2mr^2)$$

$$\dot{h}_2 = \dot{\omega}_2(I_2 + A + 2mR^2)$$

$$\dot{h}_3 = \dot{\omega}_3(I_3 + 2m\ (r^2 + R^2)) + C(\dot{\omega}_3 + \ddot{\alpha})$$

Euler's equations[15] yield

$$\dot{\omega}_1(I_1 + A + 2mr^2) + \omega_2\omega_3\ (I_3 + 2m\ (r^2 + R^2))\ C\omega_2(\omega_3 + \dot{\alpha})$$

$$- \omega_2\omega_3\ (I_2 + A + 2mR^2) = 0$$

$$\dot{\omega}_2(I_2 + A + 2mR^2) + \omega_1\omega_3\ (I_1 + A + 2mr^2) - \omega_1\omega_3\ (I_3 + 2m(r^2 + R^2))$$

$$- C\omega_1\ (\omega_3 + \dot{\alpha}) = 0$$

$$\dot{\omega}_3(I_3 + 2m(r^2 + R^2)) + C(\dot{\omega}_3 + \ddot{\alpha}) + \omega_1\omega_2(I_2 + A + 2mR^2)$$

$$- \omega_1\omega_2(I_1 + A + 2mr^2) = 0$$

$$\dot{\omega}_1(I_1 + A + 2mr^2) = \omega_2\omega_3 \{I_2 + A - I_3 - 2mr^2\} - C\omega_2 (\omega_3 + \dot{\alpha})$$

$$\dot{\omega}_2(I_2 + A + 2mR^2) = \omega_1\omega_3 \{I_3 + 2mR^2 - I_1 - A\} + C\omega_1 (\omega_3 + \dot{\alpha})$$

$$\dot{\omega}_3(I_3 + C + 2m(r^2 + R^2)) = \omega_1\omega_2 \{I_1 + 2m (r^2 - R^2) - I_2\} - C \ddot{\alpha}$$

To find an expression for $\ddot{\alpha}$, consider the friction force on the wall as in elementary pipe flow.

$$\tau_o = (f/4) \rho v^2/2$$

where 'f' is an empirical resistance coefficient. The torque then becomes:

$$N_3 = - \tau_o R_{ad} P\beta \left(\frac{|\dot{\alpha}|}{\dot{\alpha}}\right)$$

where the term in parenthesis insures that the torque acts opposed to fluid slug motion. Using an empirical friction coefficient by Blassius of

$$f = 0.316/R_n^{1/4}$$

the torque then becomes:

$$N_3 = \frac{-0.316 \rho v^2 R_{ad} P\beta}{8R_n^{1/4}} \left(\frac{|\dot{\alpha}|}{\dot{\alpha}}\right)$$

Letting

$$v = R_{ad} \dot{\alpha}$$

$$R_n = R_{ad} \dot{\alpha} D/\nu$$

$$N_3 = \frac{-0.0395\ \rho\ R_{ad}^{15/4} P\beta\ \dot{\alpha}^{1/4}\ (\frac{|\dot{\alpha}|}{\dot{\alpha}})}{(D/\nu)^{1/4}}$$

$$N_3 = \frac{-0.0395\ \rho\ R_{ad}^{15/4} P\beta\ |\dot{\alpha}|^{1/4}}{(D/\nu)^{1/4}\ \dot{\alpha}}$$

Writing the kinetic energy of the fluid slug as

$$T_s = \frac{1}{2} A\omega_1^2 + \frac{1}{2} A\omega_2^2 + \frac{1}{2} C\ (\omega_3 + \dot{\alpha})^2$$

a Lagrangian formulation can be used to relate $\ddot{\alpha}$ to the motion of the body. In the following equation, Q_α is the retarding torque, therefore

$$Q_\alpha = N_3$$

$$\frac{d}{dt} (\frac{\partial T}{\partial \dot{\alpha}}) - \frac{\partial T}{\partial \alpha} = Q_\alpha$$

$$\frac{d}{dt} (C(\omega_3 + \dot{\alpha}) = - \frac{.0395\ \rho R_{ad}^{15/4} P\beta\ |\dot{\alpha}|^{11/4}}{(D/\nu)^{1/4}\ \dot{\alpha}}$$

$$C\ddot{\alpha} = \frac{-.0395\ \rho\ R_{ad}^{15/4}\ |\dot{\alpha}|^{11/4}}{(D/\nu)^{1/4}\ \dot{\alpha}} - C\dot{\omega}_3$$

$$\ddot{\alpha} = \frac{-.0395\ \rho\ R_{ad}^{15/4} P\beta\ |\dot{\alpha}|^{11/4}}{C(D/\nu)^{1/4}\ \dot{\alpha}} - \dot{\omega}_3$$

Combining this with the equations for $\dot{\omega}$ results in the complete equations of motion for the rigid body

$$\dot{\omega}_1 = \frac{\omega_2\omega_3 \{I_2 + A - I_3 - C - 2mr^2\} - C\omega_2\dot{\alpha}}{I_1 + A + 2mr^2}$$

$$\dot{\omega}_2 = \frac{\omega_1\omega_3 \{I_3 + C - I_1 - A + 2mR^2\} + C\omega_1\dot{\alpha}}{I_2 + A + 2mR^2}$$

$$\dot{\omega}_3 = \frac{\omega_1\omega_2 \{I_1 + 2m (r^2 - R^2) - I_2\} + \dfrac{.0395\ \rho R_{ad} P\beta\ |\dot{\alpha}|^{11/4}}{(D/\nu)^{1/4}\ \dot{\alpha}}}{I_3 + 2m(r^2 + R^2)}$$

$$\ddot{\alpha} = \frac{.0395\ \rho\ R_{ad} P\beta\ |\dot{\alpha}|^{11/4}}{C(D/\nu)^{1/4}\ \dot{\alpha}} - \dot{\omega}_3$$

For the computer simulation $\dot{\alpha}$ is treated as the principle variable. Thus the preceding are four first order differential equations in four unknowns. Moving the masses to the $_1$ axis (the proposed control motion) results in the following equations:

$$\dot{\omega} = \frac{\omega_2\omega_3(I_2 + A - I_3 - C) - C\omega_2\ \dot{\alpha}}{I_1 + A}$$

$$\dot{\omega}_2 = \frac{\omega_1\omega_3(I_3 + C - I_1 - A + 2m(r + R)^2) + C\omega_1\ \dot{\alpha}}{I_2 + B + 2m(r + R)^2}$$

$$\dot{\omega}_3 = \frac{\omega_1\omega_2(I_1 - I_2 - 2m\,(r + R)^2) + \dfrac{.0395\rho R_{ad}^{15/4} P\beta |\dot{\alpha}|^{11/4}}{(D/\nu)^{1/4}\,\dot{\alpha}}}{I_3 + 2m\,(r + R)^2}$$

$$\ddot{\alpha} = \frac{-.0395\ \rho R_{ad}^{15/4}\ P\beta\ |\dot{\alpha}|^{11/4}}{C(D/\nu)^{1/4}\,\dot{\alpha}} - \omega_3$$